Articles

Molecular Modeling of the Three-Dimensional Structure of Dopamine 3 (D_3) Subtype Receptor: Discovery of Novel and Potent D_3 Ligands through a Hybrid Pharmacophore- and Structure-Based Database Searching Approach

Judith Varady,[†] Xihan Wu,[†] Xueliang Fang,[†] Ji Min,[†] Zengjian Hu,[†] Beth Levant,[‡] and Shaomeng Wang*[,†]

Departments of Internal Medicine and Medicinal Chemistry, University of Michigan, 3-316 CCGC Box 0934, 1500 East Medical Center Drive, Ann Arbor, Michigan 48109-0934 and Department of Pharmacology, Toxicology, and Therapeutics, University of Kansas Medical Center, Kansas City, Kansas 66160-7417

Received February 19, 2003

The dopamine 3 (D_3) subtype receptor has been implicated in several neurological conditions, and potent and selective D_3 ligands may have therapeutic potential for the treatment of drug addiction, Parkinson's disease, and schizophrenia. In this paper, we report computational homology modeling of the D_3 receptor based upon the high-resolution X-ray structure of rhodopsin, extensive structural refinement in the presence of explicit lipid bilayer and water environment, and validation of the refined D_3 structural models using experimental data. We further describe the development, validation, and application of a hybrid computational screening approach for the discovery of several classes of novel and potent D_3 ligands. This computational approach employs stepwise pharmacophore and structure-based searching of a large three-dimensional chemical database for the identification of potential D_3 ligands. The obtained hits are then subjected to structural novelty screening, and the most promising compounds are tested in a D_3 binding assay. Using this approach we identified four compounds with K_i values better than 100 nM and eight compounds with K_i values better than 1 μM out of 20 compounds selected for testing in the D_3 receptor binding assay. Our results suggest that the D_3 structural models obtained from this study may be useful for the discovery and design of novel and potent D_3 ligands. Furthermore, the employed hybrid approach may be more effective for lead discovery from a large chemical database than either pharmacophore-based or structure-based database screening alone.

Introduction

The dopamine 3 (D_3) receptor, cloned in 1990, has 52% sequence homology to the D_2 receptor and a similar but unique pharmacological profile. The D_3 receptor has been proposed as a potential therapeutic target for a variety of conditions, including drug abuse, restless legs syndrome, schizophrenia, Parkinson's disease, and depression.[1−4] Accordingly, major medicinal chemistry efforts have been made toward the design and development of potent, novel, and selective D_3 ligands.

A number of relatively selective D_3 ligands have been identified over the years, but very few D_3 ligands with unambiguous selectivity are available. PD 128907 (**1**) is probably the most selective D_3 agonist (or a relatively efficacious partial agonist) and has a selectivity of 98-fold between the D_3 and D_2 receptors using an antagonist as the reference radioligand.[5] 7-OH-DPAT (**2**) is the best characterized D_3 partial agonist to date and has a selectivity of 70-fold between the D_3 and D_2 receptors.[6] BP 897 (**3**) has a selectivity of 66-fold between the D_3 and D_2 receptors;[7] however, whether this compound possesses partial or antagonist activity is controversial.[8] Until recently, the most selective D_3 antagonists reported in the literature have a selectivity ratio of approximately 300 between the D_3 and D_2 receptors.[2] However, a highly D_3 selective antagonist designed based upon the core structure of BP 897 was recently reported.[9]

To date, accurate three-dimensional (3D) structural information for the dopamine receptors has not been available and the structural basis of ligand binding and selectivity to the D_3 receptor is poorly understood. Since dopamine receptors are membrane-bound proteins, experimental determination of their 3D structures is still an extremely difficult task. The lack of accurate structural information on D_3 and other dopamine receptors represents a significant impediment toward developing highly selective D_3 ligands.

Dopamine receptors belong to the family of G-protein coupled receptors (GPCRs), whose structures are characterized by seven transmembrane (TM) helices. In the past, computational homology modeling approaches have been employed to construct the 3D models of dopamine receptors using either low-resolution structures of rhodopsin or high-resolution structures of bac-

* To whom all correspondence and requests for reprints should be sent. Phone: (734) 615-0362. Fax: (734) 647-647. E-mail: shaomeng@umich.edu.
[†] University of Michigan.
[‡] University of Kansas Medical Center.

10.1021/jm030085p CCC: $25.00
Published on Web 09/03/2003

teriorhodopsin.[10−15] Since bacteriorhodopsin is not a GPCR and has very low sequence homology with the dopamine receptors, the accuracy of the dopamine receptor models based upon the structures of bacteriorhodopsin was limited. Since rhodopsin and dopamine receptors belong to the same subfamily of the GPCR proteins, the structure of rhodopsin was the choice as the template structure for modeling. However, prior to the determination of the crystal structure of rhodopsin in 2000,[16] only low-resolution rhodopsin structures were available, which also greatly limited the accuracy of modeled structures. Furthermore, due to limited computing power, structural refinement was performed without inclusion of the proper lipid and water environment that is required for accurate modeling.

The crystal structure of rhodopsin has been determined to 2.8 Å resolution through X-ray diffraction in 2000.[16] Since then, several high-resolution structures of rhodopsin have been determined.[17−20] The high-resolution structures of rhodopsin provided us with an opportunity to accurately model the 3D structures of dopamine receptors through computational homology modeling. Of note, since lipid and water environment plays an important role for the dopamine receptor structures,[21−22] we also included explicit lipid and water molecules in the molecular dynamics (MD) simulations for further structural refinement. D_3 receptor models were then validated using available experimental information, i.e., substituted cysteine accessibility method (SCAM) results, mutational data, and structure−activity relationships (SAR) of known D_3 ligands.

On the basis of the modeled D_3 receptor structures, we further applied a hybrid, stepwise computational screening approach for the discovery of novel and potent D_3 ligands. In this computational approach, a pharmacophore model was developed and used to identify potential novel D_3 ligands ("hits") from a large 3D structural chemical database of approximately 250 000 synthetic compounds and natural products. Hits identified from pharmacophore searching were further screened through structure-based searching using multiple receptor models via computational docking and scoring. Top-ranked potential D_3 ligands were further subjected to structural novelty screening. Finally, the most promising potential D_3 ligands were tested for their binding affinities to the D_3 human receptors. This approach led to the successful discovery of several classes of potent and novel D_3 ligands and may serve as further validation of our D_3 receptor structural models.

This paper is organized as follows. We first present the computational structural modeling of the D_3 receptor in explicit lipid and water environment and validation of the structural models using extensive experimental data. We next describe our discovery of structurally diverse and novel D_3 ligands through a stepwise computational database screening, followed by experimental testing of selected potential ligands.

Results and Discussion

1. Modeling of the D3 Receptor and Its Natural Environment. Modeling the Transmembrane Helices of the D_3 Receptor. The dopamine receptors and rhodopsin belong to the rhodopsin family within the GPCR superfamily. The basic structural topology of rhodopsin and dopamine receptors is shown in Chart 1, including the seven TM helices (TM1−TM7) and an additional short helical region (TM8) at the intracellular end of TM7. We used the rhodopsin structure determined at 2.8 Å resolution[16] as the template structure to model the TM helical region of the D_3 receptor that includes the ligand-binding site. A previous sequence analysis of 493 members of the rhodopsin family of GPCR proteins provided us with an unambiguous sequence alignment without gaps in the TM region between the D_1, D_2, and D_3 receptors and rhodopsin, as shown in Figure 1.[23] The sequence identity between the D_3 receptor and rhodopsin is 28%. Furthermore, the D_3 receptor contains 97% of the residues conserved within the rhodopsin family of GPCRs. Overall, the high-resolution X-ray structure of rhodopsin provides us with an appropriate template for D_3 receptor homology modeling.

Chart 1. Topology of the Dopamine Receptors

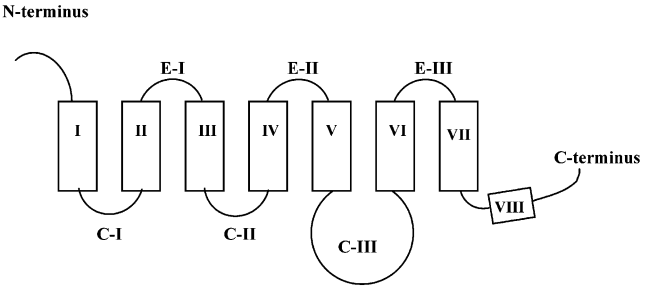

Modeling Loop Regions in the D_3 Receptor. The D_3 and other dopamine receptors contain three extracellular and three cytoplasmic loops in their structures (Chart 1). We are primarily interested in the ligand-binding site of the D_3 receptor, which is in the extracellular half of the transmembrane region. Therefore, loops that are remote from the binding site were omitted. These include the N- and C-terminus and intracellular loops C−II and C−III (Chart 1). Interchanging the C−III loop between the D_2/D_3 sequences in D_2/D_3 chimeras was found to have no effect on ligand binding affinities, which suggested that the long C−III loop may not be crucial for ligand binding.[24,25] Exclusion of these loops saved us considerable computational time in the structural refinement through extensive MD simulation. However, their omission represents a potential limitation of our current computational structural modeling of the D_3 receptor.

All extracellular loops were included. The short cytoplasmic C−I loop was also included since in the rhodopsin crystal structure this loop is in the proximity of the short helical segment TM8 and may affect the conformation of TM7. Details of loop modeling are described in the Methods section.

Modeling Lipid−Water Environment of the D_3 Receptor. The lipid membrane−water environment is important for the 3D structures of transmembrane proteins.[21,22] To further improve the accuracy of the modeled structures, we included explicitly the lipid−water environment around the D_3 receptor during structural refinement. We chose 1-palmitoyl-2-oleoyl-sn-glycero-3-phosphatidylcholine (POPC) as the lipid molecule and TIP3P water model for water molecules. POPC was chosen as the lipid molecule because it is a phosphatidylcholine lipid, the most common class of

	TM1		TM2
RHOA	W^{35}QFSML**A**AYMF**LLI**MLGFPI**N**F**L**TLYVTVQ^{64}		P^{71}L**NY**ILL**N**L**A**V**A**D**L**FMVFGGFTTTL**Y**TSLH^{100}
D_1	S^{35}VRILT**A**CFLS**LLI**LSTLLG**N**T**L**VCAAVIR^{64}		V^{58}T**N**FFVIS**LA**V**S**D**L**LVAVLVMPWKAVAEIA^{87}
D_2	P^{35}HYNYY**A**TLLT**LLI**AVIVFG**N**V**L**VCMAVSR^{64}		T^{68}T**NY**LIVS**LA**V**A**D**L**LVATLVMPWVV**Y**LEVV^{97}
D_3	R^{35}PHAYY**A**LSYCA**LI**LAIVFG**N**G**L**VCMAVLK^{64}		T^{63}T**NY**LVVS**LA**V**A**D**L**LVATLVMPWVV**Y**LEVT^{92}
	TM3		**TM4**
RHOA	P^{107}TG**CN**LEGF**F**ATLGGEIALWS**L**VVL**A**I**ERY**VVV^{139}		N^{151}HAIMG**V**AFT**WV**M**A**L**A**CAA**P**P**L**V^{173}
D_1	G^{93} SF**CN**IWVA**F**DIMCSTAS**I**LN**L**C**V**IS**V**D**RY**WA**I**^{125}		L^{153}ISFIP**V**QLS**W**HK**A**KPTSPSDGN^{175}
D_2	R^{104}IH**C**DIFVTLDVMMCTAS**I**LN**L**CA**I**S**I**D**RY**TA**V**^{136}		R^{150}RVTVMISIV**WV**L**S**FTISC**P**L**L**F^{172}
D_3	R^{100}IC**C**DVFVTLDVMMCTAS**I**LN**L**CA**I**S**I**D**RY**TA**V**^{132}		R^{148}RVALMITAV**WV**L**A**F**A**VSC**P**L**L**F^{170}
	TM5		**TM6**
RHOA	**N**^{200}ES**FVIY**MF**VV**H**F**I**IP**L**IV**I**FFC**Y**GQ^{225}		**E**^{247}**K**EV**T**R**MV**II**M**V**I**A**F**L**I**C**WL**P**YAGVAFYIFT^{277}
D_1	S^{191}RTYA**I**SSS**V**IS**F**Y**IP**VAI**M**IVT**Y**TR^{216}		**E**^{267}T**K**VLKTLSVIMGV**F**VC**CWLP**FFILNCILPF^{297}
D_2	**N**^{186}PA**FV**V**Y**SSI**V**S**F**YV**P**F**IV**TLLV**Y**IK^{211}		**E**^{368}**K**K**A**T**QM**LAIVLGV**F**I**I**C**WLP**FFITHILNIH^{398}
D_3	**N**^{185}PD**FVIY**SS**VV**S**F**YL**P**FG**V**TVLV**Y**AR^{210}		**E**^{324}**K**K**A**T**QMV**A**I**VLG**AF**IV**C**WLP**FFLTHVLNTH^{354}
	TM7		**Short TM8**
RHOA	I^{286}FMTIPAF**F**AKT**S**AVY**NPVIY**^{306}		**N**^{310}KQ**FR**NCMV**T**T**L**^{321}
D_1	N^{311}TFDVFVW**F**GWA**N**SSL**NP**I**IY**^{331}		**N**^{334}AD**FR**KAFS**T**L**L**^{345}
D_2	V^{406}LYSAFTWLGYV**N**S**A**V**NP**I**IY**^{426}		**N**^{430}IE**FR**KAFLKI**L**^{441}
D_3	E^{363}LYSATTWLGYV**N**S**A**L**NP**V**IY**^{383}		**N**^{387}IE**FR**KAFLKI**L**^{398}

Figure 1. Sequence alignment between rhodopsin (RHOA) and the D_1, D_2, and D_3 receptors in the transmembrane region yields 22%, 26%, and 28% sequence identities, respectively. Conserved residues within the rhodopsin family of GPCRs are underlined; sequence identities between rhodopsin and the dopamine receptors are in bold. These conserved amino acids combined with further sequence identities between rhodopsin and the dopamine receptors provide an unambiguous sequence alignment for each transmembrane helix. Sequence numbers are shown for first/last residues of the helices as superscripts following Swiss−Prot sequence numbering (http://us.expasy.org).

lipids in biological membranes. Also, this lipid contains an unsaturated carbon−carbon bond in one of its tails, making it a better choice for modeling biological membranes than lipids with only saturated tails. A pre-equilibrated and well-characterized structure of a POPC bilayer in liquid-crystal phase was available to model the starting lipid structure.[26] Insertion of the receptor model into the lipid bilayer is described in detail in the Methods section.

Structural Refinement of the D_3 Structure Embedded in Lipid Membrane−Water Environment. Structural refinement of the D_3 receptor with surrounding lipid−water was achieved via conformational sampling during 2.0 ns long MD simulation using the CHARMM program.[27] Structures saved in the MD simulation trajectory (2000 conformations) were analyzed primarily focusing on the ligand binding site as follows.

Conformational Cluster Analysis of the D_3 Receptor's Binding Site. The 2.0 ns long MD simulation allowed us to explore protein flexibility. We performed conformational cluster analysis to identify major conformations in the D_3 receptor structural models with respect to the binding site. D_3 receptor conformations saved in the MD simulation trajectory were first clustered based on proline kink angles in TM5 and -6. These angles affect the backbone structures of several residues important for ligand binding. The obtained conformational clusters were further clustered based on χ_1 and χ_2 side chain dihedral angles of selected residues implicated in ligand binding at various GPCRs as summarized in recent reviews,[28,29] as well as residues in their close proximity (Table 1). More details of clustering are given in the Methods section.

Conformational analysis showed that there are four major conformational clusters for the binding site based on the MD simulation trajectory, distributed as 30%, 16%, 13%, and 10% of the total conformations clustered. The conformations that represent the center conformer of these four clusters were identified and superimposed in Figure 2. The final conformer of the MD simulation (at 2000 ps) with its lipid−water environment is shown as a snapshot in Figure 3. This conformer belongs to major conformational cluster IV and therefore may be described by features characteristic of this particular group of conformers (discussed below). The four major conformational clusters of the D_3 receptor differ in average bend angles of the TM5, TM6 helices and in preferred side chain orientations of ligand-binding site residues as follows.

Considering the average kink angles of TM5 and TM6 in D_3 conformational clusters, there is no significant difference in TM5 helical bending but TM6 adopts distinct average kink angles, as given in Table 1.

Several residues in the binding site, including V111, W342, and F346, appear quite flexible and adopt different average side chain dihedral angles in the four major conformational clusters (Figure 2 and Table 1). A number of aromatic residues, including F197, W342, F345, and F346, form a hydrophobic cluster, which is accessible for ligand binding. Indeed, alanine substitutions of the residues in the D_2 receptor corresponding to F345 and F346 in the D_3 receptor were shown to affect binding of several agonists and antagonists.[30] We

Table 1. D_3 Receptor Conformations Were Clustered Based on (a) Helix 5,6 Bend Angles and (b) Side Chain Dihedral Angles of Several Residues Implicated in Ligand Binding as Well as Other Residues in Their Close Proximity

	a. conformational clusters			
helices	I	II	III	IV
TM5	16.3° ± 3.4°	16.3° ± 2.9°	15.7° ± 3.3°	14.5° ± 3.3°
TM6	32.0° ± 2.6°	32.2° ± 2.5°	39.4° ± 3.0°	38.9° ± 2.7°

b. average side chain torsional angles for major clusters I, II, III, IV

V78	174.3, 157.4, −179.7, 171.0	D110	−167.3, −166.1, −169.4, −167.3	**V111**	176.7, −59.7, −58.6, 173.4
C114	−169.6, −167.6, −169.1, −169.4	S192	−171.6, −171.6, −171.8, −173.9	S193	−61.4, −64.8, −80.4, −64.3
S196	−54.8, −56.7, −56.1, −53.1	F197	−176.4, 179.3, −176.6, −175.3	F197[a]	42.8, 42.8, 52.7, 45.0
W342	−140.5, −159.6, −161.2, −86.0	**W342**[a]	16.3, 33.2, 31.5, 12.8	F345	−179.0, 179.9, 178.2, 177.1
F345[a]	56.6, 58.5, 58.5, 54.2	**F346**	−80.4, −65.5, −66.1, −88.3	**F346**[a]	97.5, 97.0, 97.8, 71.9
T369	−60.7, −57.3, −56.1, −63.0	Y373	−66.9, −65.7, −62.5, −69.9	Y373[a]	122.6, 112.4, 117.3, 119.5

[a] γ_2. First side chain dihedral angles γ_1 are shown unless otherwise indicated. Angles were averaged per D_3 receptor conformational clusters. Features showing largest deviations between clusters (larger than 5° for kink angles or 20° for dihedral angles) are in bold.

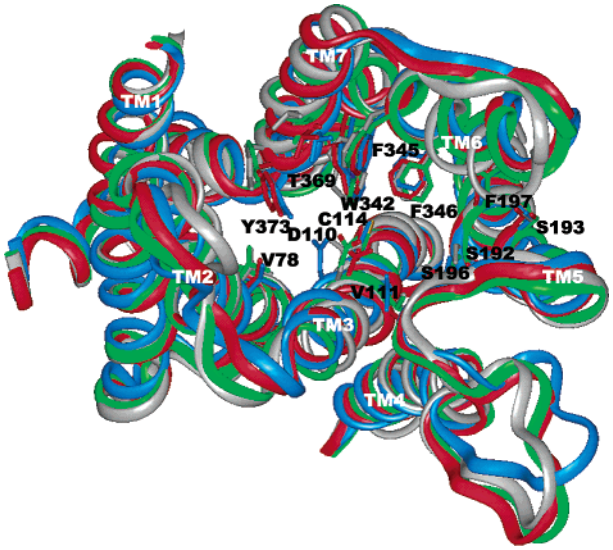

Figure 2. Four major D_3 receptor conformations obtained from 2.0 ns MD simulation. Cluster center I, II, III, and IV conformations are colored by atom, red, blue, and gray, respectively. Fitting heavy backbone atoms of each (II, III, and IV) onto the major conformer yields RMS deviations of 1.1, 1.2, and 0.8 Å, respectively, in the transmembrane region. Shown side chains were included in clustering based on dihedral angles.

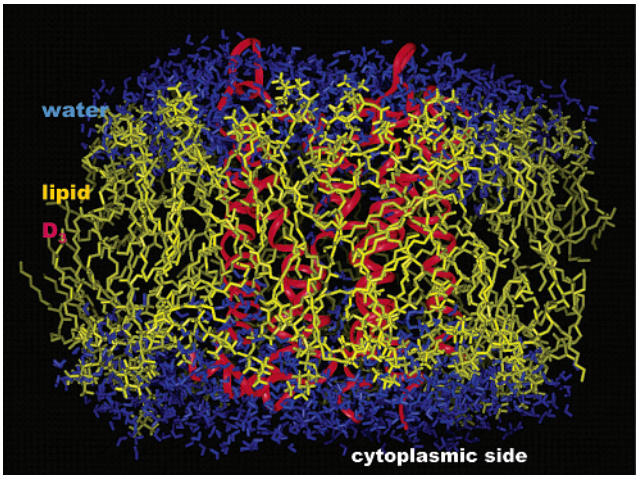

Figure 3. Snapshot of the final conformation (at 2.0 ns) of the D_3 receptor (red) also showing its POPC lipid bilayer (yellow) and water (blue) environment.

observed significant side chain conformational flexibility for W342 and F346, which might play a role in binding of the D_3 receptor to different ligands.

D_3 Models Correspond to the Inactive State of the Receptor. Our D_3 structure was modeled based on the inactive state of rhodopsin, and it was therefore expected to represent the inactive state of the receptor. Indeed, major conformational clusters have several structural features that are characteristic of the inactive state. For example, in the center conformation of the most populated conformational cluster, a salt bridge between R128 in TM3 and E324 in TM6 is formed and the distance between the centers of the guanidinium of R128 and the carboxyl group of E324 is 4.2 Å. Numerous studies have shown that in the inactive state the intracellular ends of TM3 and TM6 are in close proximity and upon activation they become more distant from each other, primarily due to the movement of TM6.[31−34] As the distance between the intracellular ends of TM3 and TM6 increases during receptor activation, the salt bridge linking these two regions is disrupted. This salt bridge is present in the inactive state of the rhodopsin crystal structure. This salt bridge was also shown to constrain the β2-adrenergic receptor in the inactive state.[35] Another characteristic of the inactive state is the burial of the TM6 cysteine residue, which corresponds to C341 in the D_3 receptor. Several studies have shown that this buried cysteine in GPCR proteins becomes exposed upon receptor activation.[36,37] Interestingly, it was shown that in the inactive state of the D_2 receptor, the adjacent residue to the TM6 cysteine residue, which is W342 in D_3, is exposed to solvent. In our D_3 receptor models, C341 is buried while the adjacent W342 is exposed to solvent. Taken together, our analysis suggests that the modeled D_3 structure is in its inactive state.

2. Validation of the 3D Structural Model of the D_3 Receptor. Regions Accessible to Solvent. Although the binding site of the D_3 receptor has not been extensively studied, the binding site of the D_2 receptor has been mapped using the substituted cysteine accessibility method (SCAM).[38−45] Considering the TM region that includes the ligand binding site, the sequence identity between the D_2 and D_3 receptors is 80%. Many ligands bind to the D_2 and D_3 receptors with similar affinities. Thus, the 3D structures of the binding sites in the D_2 and D_3 receptors should be similar and the mapped binding site information for the D_2 receptor should be applicable to that for the D_3 receptor.[38−45] On the basis of our modeled D_3 structures, D_3 residues corresponding to water-exposed residues in the large

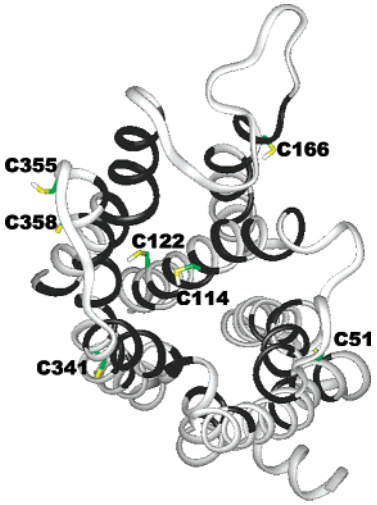

Figure 4. Water-exposed regions (black ribbon) in the transmembrane segment of the D_3 receptor as viewed from the extracellular side. Out of naturally occurring and nonbridging cysteines, only one, Cys114, was found to be exposed to sulfhydryl reagents, in agreement with the D_3 conformation cluster I center structure shown here.

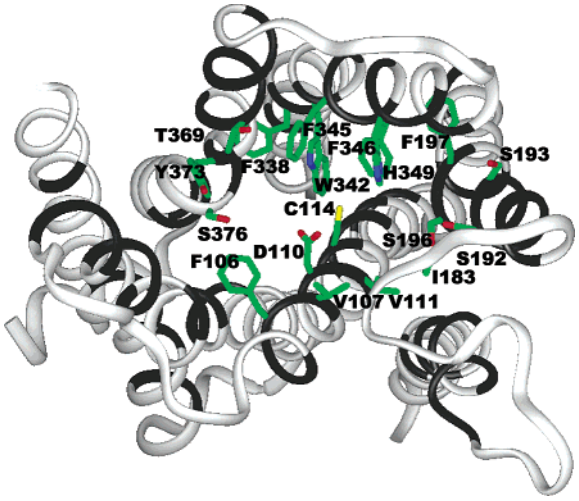

Figure 5. Subset of residues implicated in ligand binding at dopamine receptors (3.28, 3.29, 3.33, 3.36, 5.42, 5.43, 5.46, 5.47, 6.48, 6.51, 6.55, 7.39, 7.43, 7.46) and at other GPCRs (3.32, 6.44, 6.52, and residue(s) within a few amino acids following TM4−TM5 disulfide bridge) map the inside of the extracellular crevice of the most populated D_3 cluster center conformer. Helical ribbon in solvent exposed regions is colored black.

extracellular crevice formed by TM1−TM7 (the ligand binding site) in the D_2 receptor are indeed accessible to solvent (Figure 4). TM1 is furthest away from this crevice among all helices and only contributes to a pocket located deep in the TM region. Excluding bridging cysteine residues, there are two cysteine residues in the extracellular region and five cysteine residues in the TM region in the D_2 receptor corresponding to C355, C358 and C51, C114, C122, C166, C341 in the D_3 receptor. In D_2, C118 was shown to be the only cysteine residue exposed to solvent among these seven cysteine residues.[41] Indeed, in D_3, the only solvent-exposed cysteine residue among these seven cysteine residues (Figure 4) is C114, which corresponds to C118 in D_2. Thus, the D_3 receptor structure is in agreement with the SCAM experiments and with the accessibility of its naturally occurring cysteine residues to solvent. Furthermore, residues which were implicated in ligand binding at the G-protein coupled receptors using various experimental methods[28,29] are clustered within the binding pocket of the D_3 model structures (Figure 5).

Computational Docking of *R*-(+)-7-OH-DPAT into the D_3 Receptor Model. Although comprehensive docking studies of known ligands to the D_3 receptor are beyond the scope of the present study, we carried out computational studies of *R*-(+)-7-OH-DPAT to D_3 to further validate our D_3 models and to identify the residues that are involved in ligand binding. *R*-(+)-7-OH-DPAT is probably the most well-characterized D_3 partial agonist to date. Extensive structure−activity relationships (SARs) have been performed on this class of D_3 ligands. Mutational analyses have also been performed on the D_3 receptor to probe the interaction of the receptor to *R*-(+)-7-OH-DPAT. *R*-(+)-7-OH-DPAT is a partial agonist[46,47] and potently binds to both the active and inactive states of the D_3 receptor with high affinities and a slight preference to the active state.[48] As discussed above, our D_3 receptor models represent the inactive state of the D_3 receptor and may be used for computational docking of *R*-(+)-7-OH-DPAT.

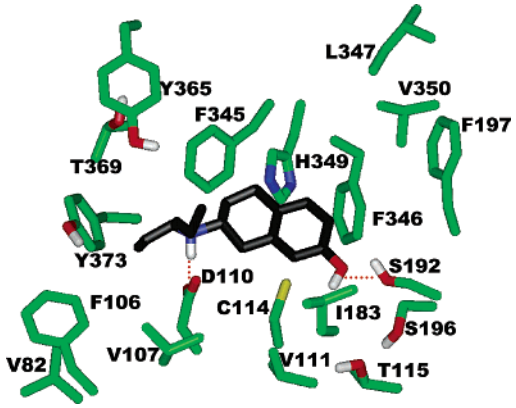

Figure 6. *R*-(+)-7-OH-DPAT docked into the binding site of the most populated D_3 cluster center conformation, as viewed from the extracellular side. Side chains within 5 Å of ligand atoms are shown. Ligand carbons are colored black; all other atoms are colored by atom type. Only polar hydrogens are shown for clarity. Orange dotted lines indicate hydrogen-bonding interactions. The salt bridge between D110 and the ligand also has a hydrogen-bonding component.

R-(+)-7-OH-DPAT was docked into all four D_3 receptor cluster center conformations using the Cerius[2] program.[49] Analysis of the predicted binding models showed that the binding mode obtained using the center conformation of the most populated cluster (cluster I) of the receptor for *R*-(+)-7-OH-DPAT (Figure 6) is consistent with all the available experimental data for this ligand, while the other predicted binding models are not entirely consistent with the experimental data. Accordingly, we focus our discussions on the binding model obtained using the cluster I conformation. Distances between heavy atom groups of the ligand and of the receptor participating in the interactions for this predicted model are summarized in Table 2.

On the basis of the predicted binding model (Figure 6 and Table 2), the protonated nitrogen in *R*-(+)-7-OH-DPAT forms a salt bridge with the negatively charged D110 while its hydroxyl forms a hydrogen bond with

Table 2. Interactions between *R*-(+)-7-OH-DPAT and D_3 Based on Binding Models Predicted Using Cerius[2] Ligandfit

interacting groups		distance	type of
(+)-7-OH-DPAT	D_3 receptor	(Å)	interaction
protonated amine	Asp110 carboxyl	2.7	salt bridge
hydroxyl group	Ser192 hydroxyl	3.6	hydrogen bonding
aromatic ring	F346 aromatic ring	5.2	aromatic
saturated part of fused ring	F345 aromatic ring	4.9	hydrophobic/steric
propyl group	T369 methyl	5.4	weak hydrophobic

[a] Distances given are between the center of mass of heavy atom groups indicated.

S192 in D_3. Several hydrophobic residues including F106, V107, V111, C114, F345, F346, and Y373 are in contact with hydrophobic groups in *R*-(+)-7-OH-DPAT. Our analysis of this binding model showed that both direct and indirect experimental data support the importance of these interactions for the binding of *R*-(+)-7-OH-DPAT to the D_3 receptor.

First, mutation of S192 to Ala (S192A) reduces the binding affinity of D_3 for *R*-(+)-7-OH-DPAT by 16-fold while the contributions of the other TM5 serines appear to be much less significant.[50] The importance of this optimal hydrogen-bonding interaction between the hydroxyl group in *R*-(+)-7-OH-DPAT and S192 is also supported by the SAR data, which showed that replacement of the hydroxyl group by a methoxyl in *R*-(+)-7-OH-DPAT reduces its binding affinity to the D_3 receptor by 100-fold.[6] Interestingly, the T369V mutant of the D_3 receptor was shown to have higher binding affinity for *R*-(+)-7-OH-DPAT than the wild-type receptor.[51] Indeed, in our predicted binding model, the methyl group of T369 is 5.4 Å away from the center of one of the propyl groups in *R*-(+)-7-OH-DPAT and mutation of T369 to valine may have improved the hydrophobic interactions between *R*-(+)-7-OH-DPAT and the receptor.

Several lines of indirect evidence also support our predicted binding model for *R*-(+)-7-OH-DPAT. F345 in the D_3 receptor corresponds to F389 in the D_2 receptor, which has been strongly implicated in ligand binding for the D_2 receptor. Mutation of F389 to alanine was shown to abolish the binding of several but not all ligands studied,[30] suggesting that this mutation may primarily affect the interactions between some ligands and the receptor rather than the overall conformation in the binding site. Residues corresponding to F345 (residue 6.51) and F346 (residue 6.52) in the D_3 receptor have been implicated in ligand binding in a number of other GPCRs. The residue at 6.51 was shown to affect ligand binding in V1a vasopressin,[52] α-1b-adrenergic,[53] and Angiotensin type I receptor.[54] The residue at 6.52 was shown to affect ligand binding in V1a vasopressin,[52] m5 muscarinic receptor,[55] and serotonin receptor.[56,57]

Taken together, our predicted binding model for *R*-(+)-7-OH-DPAT using the most populated conformational cluster (cluster I) is supported by the direct experimental data pertaining to this ligand to the D_3 receptor and indirect experimental data at other GPCR proteins.

3. Application of a Hybrid Approach for the Discovery of Novel D_3 Ligands. We employed a stepwise computational database screening approach to discover potent and structurally novel D_3 ligands, which combines pharmacophore searching[58−61] and protein structure-based searching,[62−68] followed by structural novelty screening and experimental testing (Chart 2).

Briefly, in this approach a pharmacophore model was developed based upon the structures of known D_3 ligands and used to perform a pharmacophore search from a large 3D chemical database to identify compounds ("hits") that meet the chemical and geometrical requirements specified in the pharmacophore model. These "hits" were then subjected to structure-based screening using multiple D_3 receptor conformations to identify compounds that most effectively interact with the receptor through computational docking and scoring. Top-ranked compounds from computational structure-based searching were further subjected to additional structural novelty screening in comparison to known D_3 ligands. Finally, the most promising potential D_3 ligands were selected for experimental testing of their binding affinities to the human D_3 receptor.

Deriving a Pharmacophore Model for D_3 Ligands. Ten potent and moderately selective known D_3 ligands were selected (Chart 3, compounds **1**−**10**) for the development of a D_3 pharmacophore model. Chemical structural analysis showed that these D_3 ligands contain a common aromatic ring and an sp^3 nitrogen attached to a propyl group and to two additional sp^3 carbons. The distance between the aromatic ring center and the basic sp^3 nitrogen within these compounds was found to be on average 5.16 ± 0.16 Å through conformational analysis using the QUANTA program.[69] Accordingly, a pharmacophore model was proposed, as shown in Figure 7. Of note, for the purpose of obtaining many structurally novel pharmacophore 'hits', the proposed pharmacophore model contains only a limited requirements.

Performance of Pharmacophore Searching of the NCI 3D Database. Using the pharmacophore model shown in Figure 7, we searched the latest version of the NCI 3D database of 250 251 "open" compounds[70] with the program Chem-X.[71] A total of 6727 compounds were identified as hits, which satisfy the chemical and geometrical requirements specified in the pharmacophore model.

Structure-Based Database Searching. When different ligands bind to a protein, the protein may have to adopt different conformations in order to most effectively interact with them. For this reason, we used multiple representative conformations obtained from our extensive MD simulation for structure-based searching. These 6727 "hits" obtained from pharmacophore searching were docked into each cluster center structure of the four major conformational clusters obtained from our extensive MD simulations and ranked based on the docking score function implemented in the Cerius[2] program.[49]

To test whether structure-based database searching can reasonably identify known potent D_3 ligands, we added 20 known D_3 ligands to the database of pharmacophore hits (the total number of compounds was 6747). These known ligands satisfied requirements of the pharmacophore model and showed potent binding affinities at the D_3 receptor as shown in Table 3. The radioligand used for binding affinity data of all ligands listed in Table 3 was either [^{125}I]iodosulpiride or [^{3}H]-

Chart 2. Scheme of the Hybrid Approach Applied in This Work

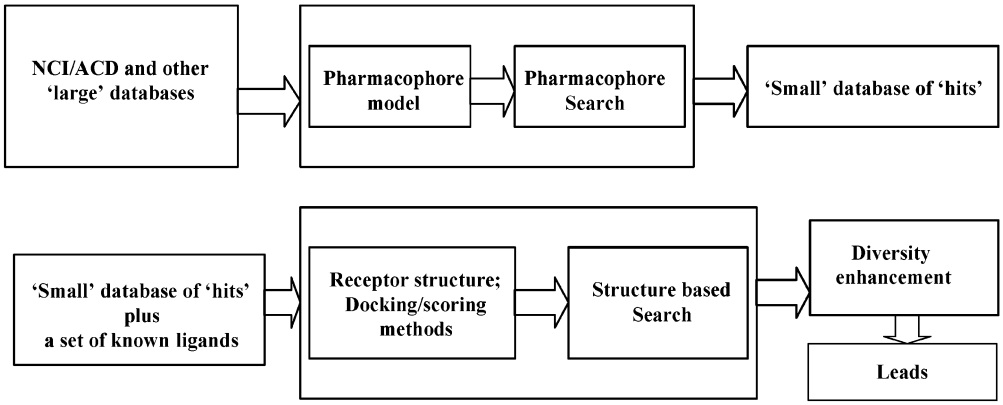

Chart 3. Chemical Structures of 10 Moderately Selective, High-Affinity D_3 Ligands Used for Developing a Pharmacophore Model for 3D Database Pharmacophore Search

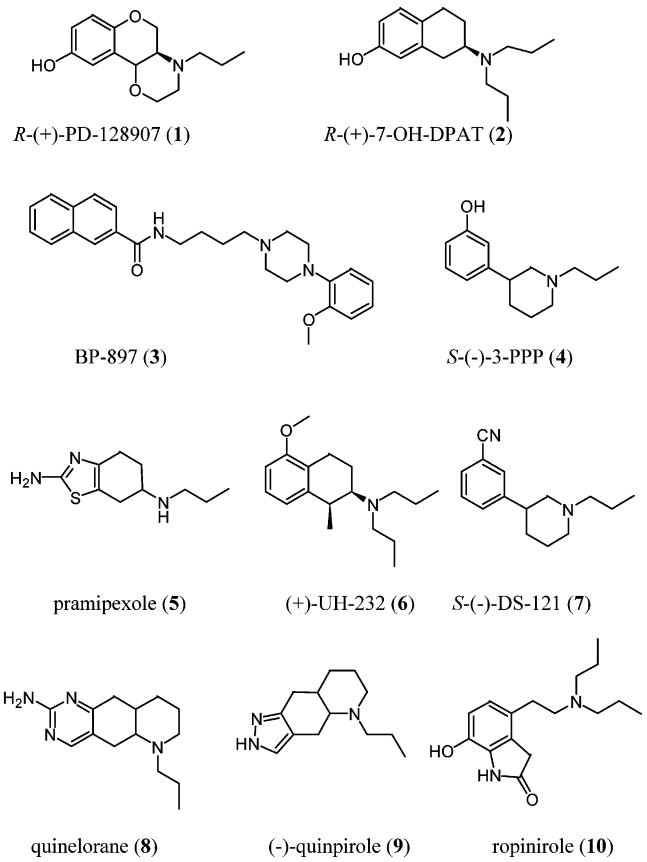

spiperone, with the exception of the otherwise highly potent ligand, eticlopride. Most ligands considered are antagonists and several of them are partial agonists. Their chemical structures cover a wide range of structural diversity (Chart 4). Since it was expected that many of these 6727 "hits" are not active, the successful identification of these 20 diverse and potent known D_3 ligands from other 6727 compounds would provide a validation to the computational docking and scoring methods used as well as the modeled D_3 receptor structures. Rank orders of these 20 known D_3 ligands based upon the docking score at each of the four D_3 cluster center conformers (either of the conformers I−IV) are shown in Figure 8.

Figure 8 also shows the rank orders of these 20 known ligands if the highest rank for a ligand is considered among any of the four receptor conformers (thin cyan line). Thus, if the highest rank is used for each ligand among the docking and scoring results using all four receptor conformers, then these 20 known compounds are ranked within the top 30% of the database of pharmacophore hits. Furthermore, 19 known D_3 ligands also rank in the top one-third of all the 6747 compounds simultaneously at least at two or more receptor conformers (thick cyan line). The latter rank order is shown in Table 3 for known D_3 ligands and also for selected database compounds in Tables 4 and 5. Using this rank order, 2478 or 37% of all pharmacophore hit compounds were found to rank in the top one-third at two or more receptor conformers.

To further improve our chance to identify truly structurally novel D_3 ligands, the set of 2478 compounds was compared to the known D_3 ligands to determine the structural similarity using an in-house program as described in the Methods section. After eliminating compounds with Tanimoto structural similarity index of greater than 80% to any of the known D_3 ligands, the remaining 1314 compounds were then considered as the most promising potential D_3 ligands from the original 250 251 NCI "open" compounds.

To date, we requested samples of 60 compounds (selected out of the total 2478 compounds) from the National Cancer Institute and 20 compounds were available with sufficient quantity for testing their binding affinities to the D_3 receptor. The chemical structures of these 20 compounds are provided in Chart 5. The rank order of these 20 compounds is provided in Table 4.

Testing of the Most Promising Potential D_3 Ligands in the Receptor Binding Assay. Binding affinities of the selected 20 potential D_3 ligands were tested using cell lines transfected with the D_3 human dopamine receptor.[72] [^{3}H]YM-09151-2, which has a high affinity to the D_3 receptor, was used as the radioligand for the D_3 receptor binding assay. Candidate compounds were measured for their ability to compete with [^{3}H]-YM-09151-2 binding to the D_3 receptor using CHO cells transfected with human D_3 (hD_3) receptors. Compounds were first screened at 10 μM. If sufficient binding was found for a compound, its IC_{50} was determined and its K_i value calculated according to the Cheng−Prusoff equation assuming classical competitive inhibition.[73]

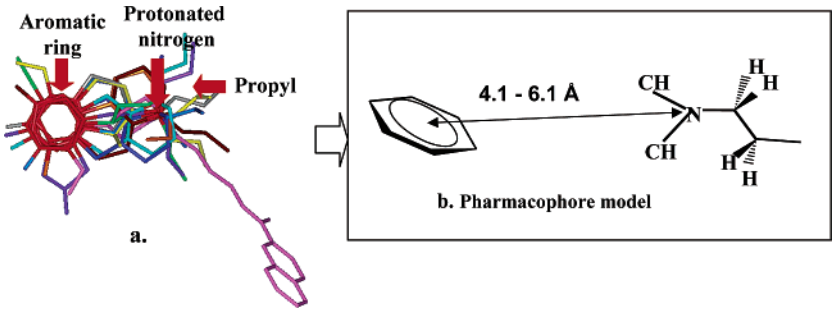

Figure 7. Deriving a pharmacophore model from known D_3 ligands: (a) Superposition of 10 D_3 partial agonists and agonists; (b) A pharmacophore model derived from these D_3 ligands.

Table 3. Binding Affinities and Rank Order of a Set of Known D_3 Ligands[a]

ligand	K_i (nM)	ref	rank (%)	ligand	K_i (nM)	ref	rank (%)
11 chlorpromazine	3.0[b]	80	5.5	**2** *R*-(+)-7-OH-DPAT[c]	2.2[b]	83	23.6
12 clozapine	88[b]	80	10.1	**4** *S*-(-)-3-PPP[c]	132[d]	72	23.7
13 metoclopramide	27[b]	81	10.8	**21** L-741,626	87[d] 60[b]	88	25.1
14[b]	2.4[d]	82	11.0	**22** domperidone	3.5[b]	85	26.0
15 sulpiride	8.0[b]	80	12.8	**23** CI-1007[c]	16.6[d]	89	26.7
16 nafadotride	0.81[b]	83	13.9	**24** spiperone	0.25[b]	86	27.7
17 raclopride	3.7[d]	84	14.1	**25** *R*-(+)-S14297	13.0[b]	86	32.5
18 (1*S*,2*R*)-AJ-76	70[b]	85	15.3	**7** *S*-(-)-DS121	249[d]	90	33.1
19 haloperidol	2.2[b]	86	18.9	**1** *R*-(+)-PD128907[c]	1.1[d]	5	33.2
20 eticlopride	0.16[e]	87	23.3	**26**	27[d]	91	35.9

[a] Given rank orders correspond to scores at two or more D_3 conformers, as shown in Figure 8. For example, spiperone ranks on top 27.7% at the center conformer of D_3 conformational cluster II and 27.1% at cluster III. The listed 27.7% value therefore covers the rank order given by both scores, between 0% and 27.7%. All ligands are antagonists except for a few partial agonists as indicated. [b] [^{125}I]iodosulpiride radioligand. [c] Partial agonist. [d] [^{3}H]spiperone. [e] [^{125}I]NCQ298 radioligands.

The results are summarized in Table 4. Out of the 20 compounds tested, compounds **27**−**30** have K_i values of less than 100 nM, compounds **31**−**34** have K_i values between 1 μM and 100 nM, and compounds **35**−**37** have K_i values between 1 and 10 μM. Compounds **38**−**45** have no appreciable binding at 10 μM. Compound **46** has no appreciable binding at 1 μM, and this compound was not tested at higher concentration due to its poor solubility.

Therefore, our computational searching combining pharmacophore-based screening followed by structure-based screening using multiple receptor conformations led to the identification of several classes of novel and potent D_3 ligands. In total, 11 out of 20 compounds show significant binding affinity, 8 compounds have K_i values less than 1 μM, and 4 compounds have K_i values than less 100 nM in the binding assay.

Testing of Other Potential D_3 Ligands with Lower Ranking in Structure-Based Screening. To test whether structure-based screening is indeed effective in improving our chance to identify potent D_3 ligands, we obtained an additional 8 structurally novel compounds that ranked lower than the 20 compounds tested by selecting from the next one-third in the ranking order of best to worst scores. We tested the binding of these eight potential ligands to the D_3 receptor under the same assay conditions. Out of these eight compounds, two compounds (**47** and **48**) have K_i values of 1.3 and 1.4 μM, respectively. The other six compounds have no appreciable binding affinity to the D_3 receptor at 10 μM. The chemical structures of these eight compounds are shown in Chart 6, and their K_i values to the D_3 receptor are provided in Table 5. Therefore, these eight potential D_3 ligands with lower ranks in the structure-based screening in general have lower affinities to the D_3 receptor, and only two compounds display any significant binding affinity to the D_3 receptor.

Advantages and Disadvantages of the Computational Database Searching Strategy Employed in This Study. The stepwise approach applied in this paper aims at overcoming some of the limitations of current pharmacophore searching and structure-based searching methods for the discovery of lead compounds. Certain advantages and disadvantages are associated with this approach, as discussed briefly below.

Although it is theoretically possible to identify the most promising ligands from a large chemical database using computational structure-based database searching alone, two conditions must be met. First, the computational docking method employed must be able to predict accurately the binding model for each compound in the database. Second, the scoring function needs to be able to predict reliably the binding affinity for each compound based upon predicted binding models, which is not satisfactory.[74] In practice, for structure-based screening of a large chemical database (e.g., hundreds of thousands of compounds), fast computational docking methods must be used, which inevitably leads to much less accurate binding mode predictions. Using pharmacophore searching as the first filter significantly reduces the number of compounds for computational structure-based screening and allows the use of computational docking methods that are more accurate but may be much slower.

Pharmacophore searching has been very effective in the discovery of novel lead compounds. A pharmacophore model with too stringent geometrical and chemical requirements often leads to very few potential ligands, even from a large database. On the other

Chart 4. 2D Chemical Structures of Known D_3 Antagonists/Partial Agonists Used for Validation of Hybrid Database Searching Strategy

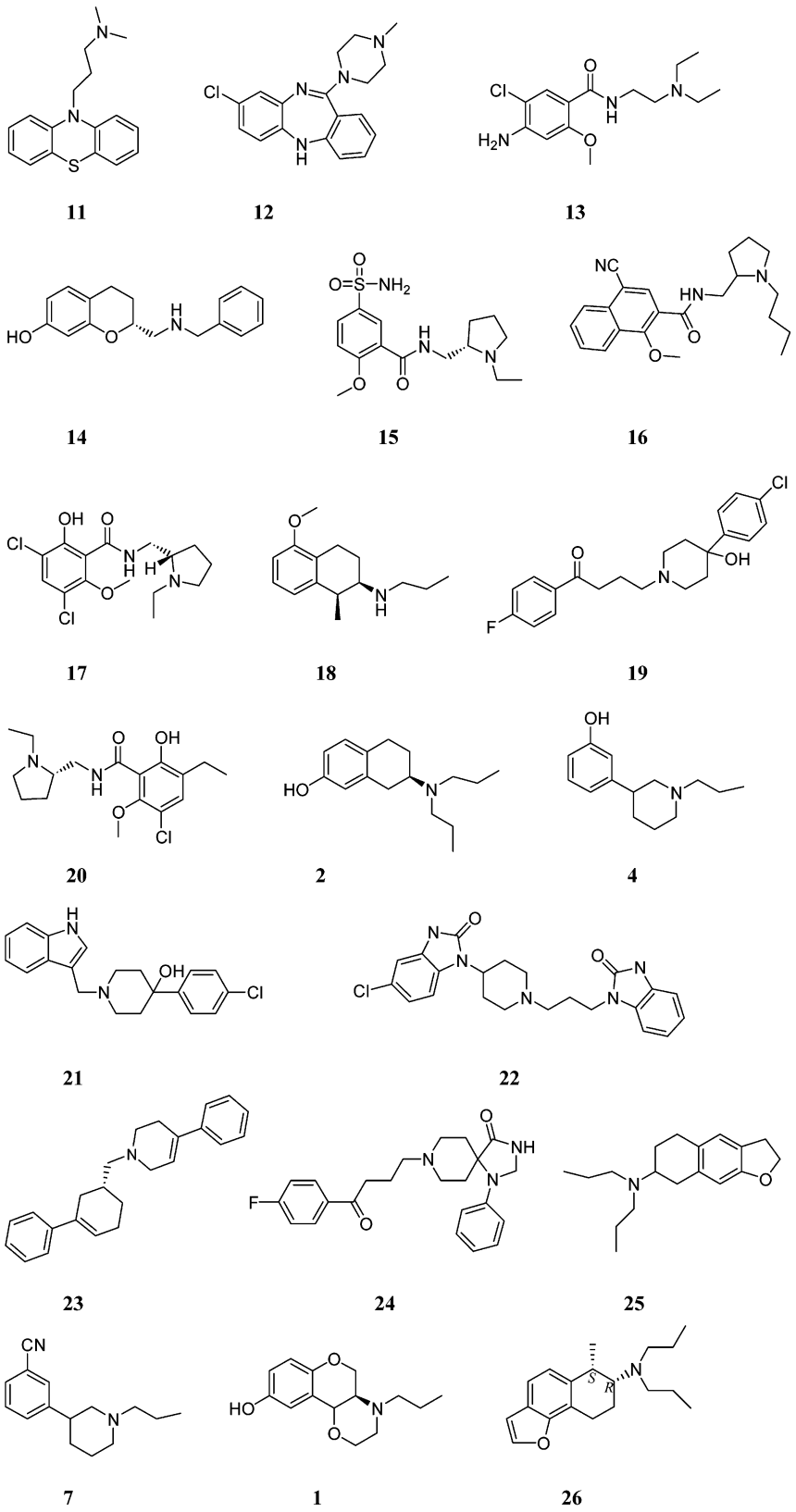

hand, the drawback of using only few and less restrictive pharmacophore requirements is that many compounds in a large chemical database will satisfy the pharmacophore model. A large percentage of these compounds will be inactive. In our approach, "hits" identified from pharmacophore searching are further screened using computational structure-based screening by evaluating the interactions between each hit and the receptor. Thus, many compounds which are unable to effectively interact with the receptor are excluded or

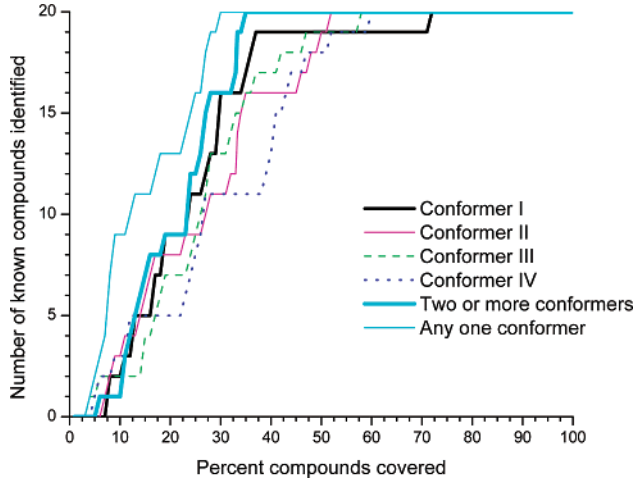

Figure 8. Recognition of known D_3 ligands out of compounds obtained from pharmacophore-based database searching plus 20 additional known D_3 ligands. 'Random' recognition would correspond to the $x = y$ line. Selection of known D_3 ligands is shown in the following cases: if structure-based searching is performed using only one receptor structure (either of the conformers I−IV), at all four receptor conformers (thin cyan curve) and two or more receptor conformers simultaneously (thick cyan line).

Table 4. Rank Orders of 20 Tested Database Compounds That Rank in the Top One-Third in Two or More Receptor Conformations Are Shown, Analogously to the Ranks Given in Table 3[a]

		rank at each D_3 conformer					
	NCI no.	I (%)	II (%)	III (%)	IV (%)	rank (%)	$K_i \pm$ SD (nM)[b]
27	143691	1.5	0.8	3.1	0.5	0.8	11.0 ± 0.6
28	131405	8.6	39.1	17.4	10.0	10.0	83.5 ± 7.3
29	170979	30.3	63.8	16.0	59.4	30.3	43.2 ± 16.7
30	309710	6.1	9.7	4.3	23.1	6.1	62.7 ± 22.4
31	24116	71.1	15.7	12.0	10.7	12.0	442 ± 62
32	147865	15.7	34.4	26.9	21.0	21.0	465 ± 83
33	147980	19.0	41.0	18.1	22.1	19.0	297 ± 90
34	167762	46.9	19.9	23.3	48.4	23.3	429 ± 42
35	402703	24.9	5.1	21.3	77.4	21.3	1381 ± 466
36	349646	2.0	10.5	10.8	1.3	2.0	2412 ± 233
37	186753	51.8	27.7	28.1	32.8	28.1	2615 ± 358
38	13636	15.5	6.8	2.5	17.4	6.8	>10000
39	22808	6.7	9.5	9.1	6.1	6.7	>10000
40	201722	4.3	5.5	2.1	21.8	4.3	>10000
41	202072	29.9	56.2	55.2	20.6	29.9	>10000
42	246981	7.0	24.0	34.0	1.3	7.0	>10000
43	298248	1.6	0.7	2.8	3.9	1.6	>10000
44	300859	37.5	24.0	12.3	38.4	24.0	>10000
45	349645	2.5	10.1	2.4	8.1	2.5	>10000
46	330803	12.6	24.1	4.4	33.0	12.6	>1000[c]

[a] Rank orders corresponding to docking/ranking at each D_3 conformer (cluster I−IV centers) are also listed. Binding affinities (K_i values) given were measured at the D_3 receptor using a cell line transfected with the human D_3 receptor. [b] Standard deviation for each compound was obtained in 2−3 experiments. [c] Due to its pure solubility, the highest concentration tested for this compound was 1 μM.

receive lower priorities in experimental testing. Furthermore, potential ligands with top ranking are further screened for their structural novelty by comparing to known ligands. This stepwise process thus identifies potential ligands that meet several criteria simultaneously: (1) all these potential ligands meet the pharmacophore requirements specified in the pharmacophore model; (2) they can effectively interact with the receptor; and (3) they are structurally novel. This process significantly improves our chance to discover potent and structurally novel lead compounds by testing only a limited number of potential ligands, as demonstrated in our current study.

Table 5. Rank Orders of Eight Tested Database Compounds That Rank in the Next One-Third (33−66%) at Two or More Receptor Conformations Are Shown, Analogously to the Ranks Given in Table 3[a]

		rank at each D_3 conformer					
	NCI no.	I (%)	II (%)	III (%)	IV (%)	rank (%)	$K_i \pm$ SD (nM)[b]
47	14232	65.3	43.2	60.3	55.7	55.7	1258 ± 419
48	24115	68.5	46.0	41.5	73.6	46.0	1419 ± 223
49	13044	59.7	49.0	55.1	58.4	55.1	>10000
50	167769	61.1	39.7	11.9	36.8	36.8	>10000
51	170980	62.4	58.6	32.6	57.1	57.1	>10000
52	265314	73.5	37.1	11.7	46.6	37.1	>1000[c]
53	362648	37.1	51.3	52.3	19.9	37.1	>10000
54	647422	43.8	40.6	62.7	49.0	43.8	>10000

[a] Rank orders corresponding to docking/ranking at each D_3 conformer (cluster I−IV centers) are also listed. Binding affinities (K_i values) given were measured at the D_3 receptor using a cell line transfected with the human D_3 receptor. [b] Standard deviation for each compound was obtained in 2−3 experiments. [c] Due to its pure solubility, the highest concentration tested for this compound was 1 μM.

Compared to structure-based database searching alone, a potential drawback of this stepwise screening approach is that the bias introduced by the pharmacophore model is carried to the structure-based screening step. Thus, some structurally novel ligands that do not meet the pharmacophore requirements specified in the pharmacophore model are excluded. To minimize this potential drawback, we used a pharmacophore model that imposed minimal chemical and structural constraints in our current study. Another possible solution to overcome this drawback is to use multiple pharmacophore models for pharmacophore searching and combine the obtained pharmacophore hits for the following step structure-based searching.

Summary

In this paper, we presented our computational modeling of the human D_3 receptor structure based upon the high-resolution X-ray structure of rhodopsin and validation of the modeled structures using experimental data. We demonstrated that our modeled structures are consistent with existing experimental data with respect to the ligand-binding site of the D_3 receptor.

We next presented our development and application of a stepwise and "hybrid" computational approach to discover novel D_3 ligands. Using this approach, we were able to discover 4 compounds with K_i values better than 100 nM and 8 compounds with K_i values better than 1 μM out of 20 compounds selected for testing in the D_3 receptor binding assay. Testing of eight other compounds that had lower ranks in structure-based screening only led to the identification of two moderately active ligands with K_i values of approximately 1μM but no potent ligands. Taken together, our results demonstrate that the employed stepwise, hybrid computational screening approach may be more effective for discovering potent and structurally diverse ligands from a large chemical database than either pharmacophore-based or structure-based database screening alone.

Chart 5. 2D Structures of 20 Tested Compounds Ranking on the Top One-Third at Two or More D_3 Receptor Conformations Based upon the Results of Structure-Based Searching

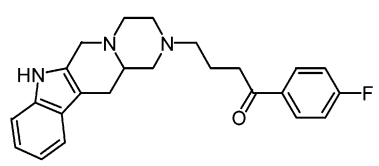

27

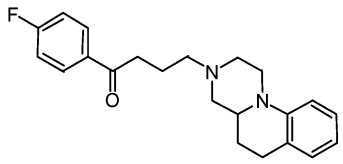

28

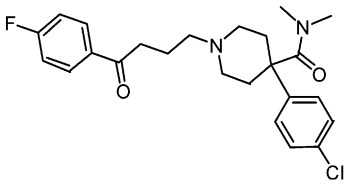

29

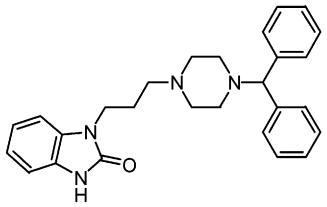

30

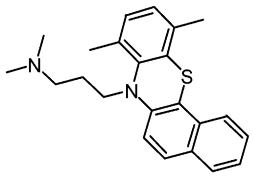

31

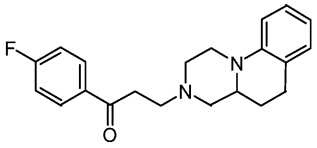

32

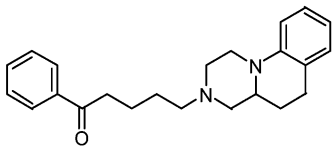

33

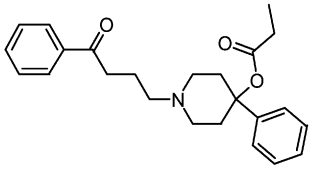

34

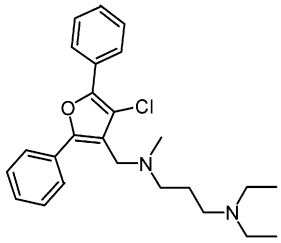

35

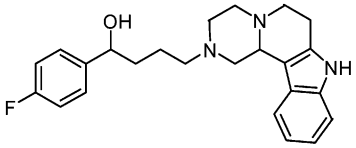

36

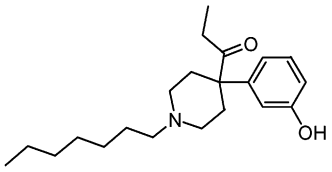

37

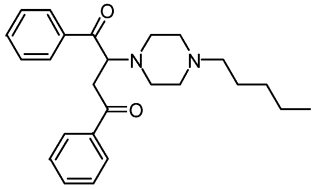

38

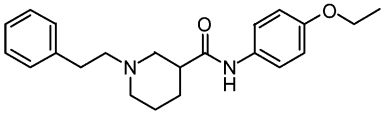

39

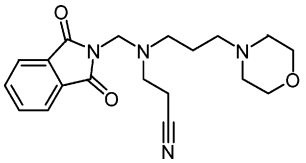

40

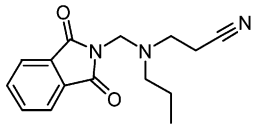

41

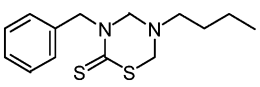

42

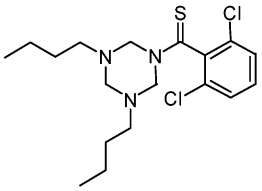

43

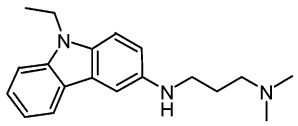

44

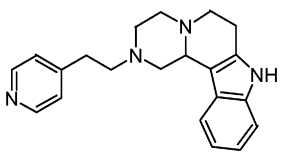

45

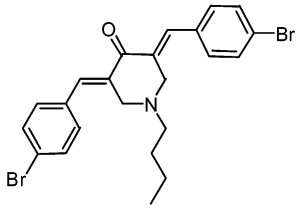

46

Chart 6. 2D Structures of Eight Tested Compounds Ranking below the Top One-Third (within 33−66%) at Two or More D_3 Receptor Conformations

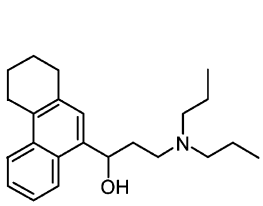

47

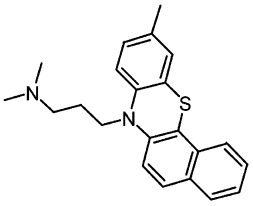

48

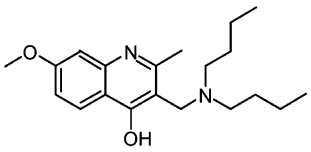

49

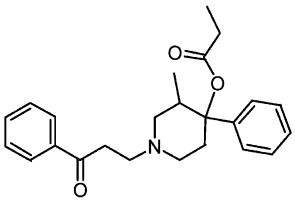

50

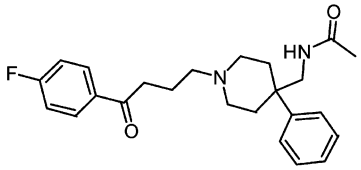

51

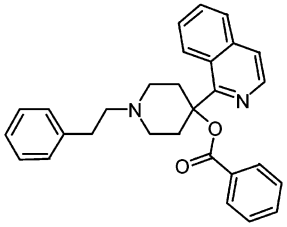

52

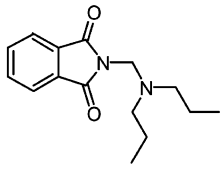

53

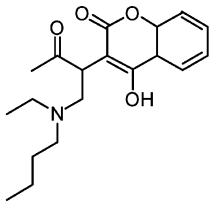

54

Methods

Computational Homology Modeling and Model Refinement. D_3 Transmembrane Helices. The transmembrane region of the D_3 receptor was homology modeled based on a 2.8 Å resolution rhodopsin crystal structure.[16] The sequence alignment used has been previously described between rhodopsin and rhodopsin family GPCRs[23] and shown on Figure 1 between rhodopsin and the D_1, D_2, D_3 subtype dopamine receptors. The sequence identity between the D_3 and rhodopsin sequence is 28% in the transmembrane region.

There are three conserved proline residues in TM5, -6, and -7 in rhodopsin that significantly bend the helices. These three important prolines are conserved among rhodopsin and dopamine receptors. Thus, these kinks in the D_3 receptor can be accurately modeled. Excluding prolines within a few residues of helical ends, there are two additional prolines in rhodopsin that correspond to residues other than proline in D_3: Pro53 in TM1 and Pro291 in TM7 of the rhodopsin sequence corresponding to Phe45 and Thr368 in D_3 (Figure 1). Hence, a normal helical conformation should be maintained in these two positions in the D_3 structure. Thus, in our modeling, weak NOE restraints were applied during an initial MD simulation between backbone atoms in these two positions until a normal hydrogen-bonding pattern of α-helix was formed. No special treatment was applied to Pro84 (TM2) in D_3, which is Thr92 in rhodopsin. The lack of backbone hydrogen bonding in D_3 at this position is expected to affect the backbone structure differently during equilibration than if residue 84 of D_3 sequence were a non-proline amino acid. The local conformational sampling performed during equilibration was sufficient to relax TM2 of the D_3 structure into a helical bend of 28.5° at Pro84. The bend angle of TM2 was maintained around this value during the production run; the most populated conformational cluster center conformer contains a TM2 bend of 27.3°, while in the final conformer (at 2.0 ns) TM2 is bent at 30.8°.

D_3 Loops. The following loop regions show significant sequence identity between D_3 and rhodopsin, and therefore, these loops were also homology modeled based on the rhodopsin crystal structure: C−I (33%), E−I (33%), and E-III (25%). For the E-II loop, there is no significant sequence homology between rhodopsin and D_3; however, the C103−C181 disulfide bridge connecting the E-II loop and TM3 greatly reduces the number of low-energy conformations. We have attempted to model this loop structure by generating possible structures that satisfy the spatial requirements of the disulphide bond

between C103−C181 and at the same time occupy approximately the same region in the D_3 model structure as in rhodopsin.

Modeling the Environment of the D_3 Receptor. A bilayer of 200 1-palmitoyl-2-oleoyl-sn-glycero-3-phosphatidylcholine (POPC) lipid covered with water on the intra- and extracellular sides was used as starting structure of the protein's environment.[26] For all MD simulations, energy minimizations, and structural analysis of the protein and environment, the CHARMM program[27] (version 27) was used. The CHARMM force field[75,76] was applied to all the protein and lipid atoms except that for the POPC lipid hydrocarbon tails united atom model was chosen. Water molecules were based on the TIP3P water model.

The D_3 receptor does not have a regular shape, and therefore, simply inserting it into a hole created within the membrane model would cause severe van der Waals repulsion in certain regions while leaving voids in other regions between the protein and the lipid. To overcome this problem, the D_3 receptor model was inserted gradually into the lipid bilayer as follows. First, a hole with an approximate diameter of 18 Å was created by deleting lipid molecules. Next, the size of the protein structure was scaled down by 50% and placed at the center of this hole according to the position of the predicted membrane boundaries obtained from the sequence analysis of about 500 rhodopsin family GPCRs.[23] The protein structure was then gradually scaled to its original size in 5% incremental steps of the van der Waals radii of atoms. At each step, nested energy minimizations and short MD simulation runs (25 ps simulation time per increment) were used, during which the lipid molecules were allowed to adjust themselves to accommodate the protein structure while the protein was kept rigid. The total accumulated simulation time over 11 cycles was 275 ps. Finally, the environment was trimmed down to a 2−3 lipid layer thickness around the protein, which yielded a total of 76 lipid molecules and 1000−1200 waters on each face of the lipid bilayer. The size of the system is 16210 atoms.

Structural Refinement of the D_3 Receptor and Its Environment. The system containing the D_3 receptor and its lipid−water environment was equilibrated using nested energy minimizations followed by short molecular dynamics simulation (MD) runs. Energy minimizations employed the adopted-basis Newton Raphson method, and for MD simulations the Leapfrog Verlet algorithm of the CHARMM program was used. To reduce artifacts caused by a layer of lipid molecules at the edges lacking their 'outer' neighbors, the stochastic boundary method was applied if hydrocarbon tail atoms were further than 33 Å away from the origin; the friction coefficient was set to 200. The phosphorus atoms in the lipid headgroups were fixed, except for lipids within 5 Å of the protein, where the lipid headgroups were instead very weakly restrained to their original position using harmonic restraints (force constant between 0.8 and 8 kcal/mol/Å^2). The dielectric constant was set to 1 and the time step to 1 fs. The temperature was kept constant at 300 K with a coupling decay time of 1.0 ps. Long-range electrostatic forces were treated with the force switch method in the range of 12−14 Å; van der Waals forces were cut at 14 Å. The nonbond list was generated up to 15 Å and updated heuristically. The frequency of checking atoms entering the Langevin region was set to 20 steps. Trajectory files of the final production runs containing coordinates were saved every picosecond. During equilibration in the first 250 ps of simulation time, weak NOE restraints were applied at backbones of F45 and T368. These two D_3 residues were aligned with two proline residues in the rhodopsin sequence and the restraints served to enforce backbone hydrogen-bonding characteristic of the α-helix. After removing the NOE restraints, MD simulation was performed for another 100 ps long run. The production MD simulation run was 2.0 ns long using the same setup as in the last 100 ps of equilibration. All computations were done using a 32 CPU origin 2000 at the National Institute of Health (NIH).

Conformational Clustering of the D_3 Receptor's Binding Site. Conformers saved during the first 0.5 ns were skipped, and clustering was over the last 1.5 ns MD simulation time (or 1500 conformations). Conformational clustering was done in two steps. In the first step TM5, TM6 bend angles were calculated for each conformer. These values were clustered using the command 'cluster' within the Correl facility of the CHARMM program, which was intended for clustering time series data. The clustering algorithm was based on a self-organizing neural net.[77,78] The following 'cluster' command parameters were used: 'angle' to indicate that the values used for clustering are angles, the maximum cluster radius was set to 10. All other parameters were default values. The obtained two clusters were further subdivided in the second step based on side chain dihedral angles of residues listed in Table 1.b: χ_1 and in case of the bulkiest side chains χ_2 also. In this step clustering was based on 18 side chain dihedral angle value series using the following 'cluster' command parameters: 'angle' to indicate that the values used for clustering are angles, with the maximum cluster radius set to 30. All other parameters were default values. The number of conformers that belonged to each cluster obtained in the second step was expressed as the percentage of the total number of conformers (1500): 30.3%, 16.0%, 13.1%, 10.0%, and several further clusters with much lower number of conformer memberships. Each cluster is characterized by the average values of TM5, TM6 bend angles and the 18 side chain dihedral angles used for second-step clustering. We defined 'cluster center conformers' as those conformations that have TM5, TM6 bend angle and the side chain dihedral angles simultaneously closest to the cluster averages. For each of the four cluster center conformer, we found a particular cluster center conformer that was closer than others to cluster averages, and therefore, this conformation was selected as the 'center' conformer, although in other cases multiple 'centers' may also be selected. Scripts and short accessory programs were used to assist in various simple tasks, for example, in pinpointing cluster center conformations out of the structures in the MD simulation trajectory.

Pharmacophore Model Building. A conformational search was performed for 10 potent D_3 ligands by systematic rotation of nonring single bonds in 30° increments, followed by 1000 steps of adopted-basis Newton Raphson (ABNR) energy minimization at each increment. The obtained conformers were clustered into groups using a root-mean-square-deviation (RMSD) value of 1.0 Å of heavy atoms, and the lowest energy conformer was retained per cluster for each molecule. First, the most conformationally constrained structures, followed by conformers of the remaining compounds, were overlaid to maximize common structural features among these ligands. We found that at least one conformer for each compound fits a common pharmacophore, as depicted in Figure 7. The modeling program Quanta (versions 97 and 98)[69] was used for all computations discussed above.

Pharmacophore-Based Database Searching. The program Chem-X with default parameters was used for all pharmacophore searching. The protonation states of the obtained pharmacophore 'hits' were adjusted to correspond to pH7.4.

Structure-Based Database Searching and Scoring. Structure-based database searching was performed using the 'Ligand Fit' module of the program Cerius^2 (version 4.6).[49] The grid used for defining the protein's binding pocket was generated based on the protein's shape using default values except that the radii of all atoms were set to 2.0 Å. Regions closer to the intracellular side or within the intra- or extracellular loops were excluded (since the binding site is believed to be in the extracellular crevice of the protein). The CFF force field (version 1997) was used as implemented into Cerius^2 (version 4.6). Ligand docking into the binding site was performed using the Monte Carlo method for conformational search; the number of trials was set to 10000, and the maximum number of ligand conformers saved to 100. Flexible docking and soft potential interaction energy between receptor and ligand were chosen with default penalties for atoms outside of the binding site. The ligands were not energy minimized after docking. Cluster-

ing of ligand conformations was done using default parameters. Docked ligands were scored based on Cerius[2] 'dock score' that approximates the negative of the receptor−ligand potential interaction energy. Docking *R*-(+)-7-OH-DPAT was done using Cerius[2] (version 4.6) Ligand fit module with the same specifications as for structure-based database searching, except that the number of trials of the Monte Carlo conformational search was increased to 0.99×10^6. Considering the top 10% scoring binding modes; a single binding mode is predicted for *R*-(+)-7-OH-DPAT.

Structural Similarity Searching. The structural diversity search was done using an in-house program. Briefly, for each compound, binary fingerprints (1024 bits) were generated using a hashing algorithm and stored in a database. The following equation was used to measure the 2D structural diversity of two molecules.[79]

$$D = 1 - S$$

$$= 1 - \frac{N_{A\&B}}{N_A + N_B - N_{A\&B}}$$

S is the Tanimoto coefficient; N_A and N_B are the number of bits set in the fingerprints of molecule A and B, respectively, $N_{A\&B}$ is the number of bits that are set in both molecules.

Determination of Ligand Binding Affinities to the D_3 Receptor. Twenty-eight compounds were measured for their ability to compete with [^{3}H]YM-09151-2 binding to the D_3 receptor using CHO cells transfected with human D_3 (hD_3) receptors. CHO cells transfected with human D_3 (hD_3) receptors were grown to confluence in α minimum essential medium (α MEM) containing 10% fetal calf serum, 0.05% pen-strep, and 600 μg/mL of G418. The cells were scraped from the 100 × 20 mm plates and centrifuged at 500 × *g* for 5 min. The pellet was homogenized by polytron in 50 mM Tris-HCl, pH 7.7, and centrifuged at 27000 × *g* for 12 min. The pellet was resuspended in 50 mM Tris, D_2 at 5 mg of protein/mL, D_3 at 1 mg of protein/mL, and stored at −70 °C in 1-mL aliquots.

On the day of the experiment, CHOp-D_3 cells were thawed, resuspended in 50 mM Tris, and centrifuged at 27000 × *g* for 12 min. The pellet was then resuspended at 1 mg of protein/80 mL in 50 mM Tris containing 120 mM of NaCl, 5 mM of KCl, 1.5 mM of $CaCl_2$, 4 mM of $MgCl_2$, and 1 mM of EDTA, pH7.4. Then 0.8 mL of cell homogenate (0.01 mg of protein/well) was added to wells containing 100 μL of the test drug or buffer and 100 μL of [^{3}H]YM-09151−2 (0.21 mM final concentration). Nonspecific binding was determined with 1 μM of chlorpromazine. The plates were incubated at 25 °C for 60 min before filtration. The filters were soaked in 0.1% PEI before filtering. Bound radioactivity was counted using a scintillation counter. Each drug was first screened at 10 μM. If more than 50% of inhibition was observed, six drug concentrations were tested to determine its IC_{50} value and its K_i value was calculated according to the Cheng−Prusoff equation assuming classical competitive inhibition.

Acknowledgment. We greatly appreciate the National Institute on Drug Abuse, National Institutes of Health (NIH), for their collaboration on testing the compounds presented in this study for their binding affinities to the human D_3 receptors under NIDA N01 DA-7-8072 "Receptor activity testing for medication discovery". The help from Dr. James Biswas and Dr. Richard Kline at the National Institute on Drug Abuse, NIH, on this project is also greatly appreciated. Initial chemical samples for compounds **27**−**54** were provided by the Drug Synthesis & Chemistry Branch, Developmental Therapeutics Program, National Cancer Institute, NIH, and their help on this project is highly appreciated.

Note Added after ASAP Posting. This manuscript was released ASAP on 9/3/2003 with structures for **35**−**46** missing from Chart 5 and with incorrect units in footnote c of Tables 4 and 5. The correct version was posted on 9/15/2003.

References

(1) Joyce, J. N. Dopamine D_3 receptor as a therapeutic target for antipsychotic and antiparkinsonian drugs. *Pharmacol. Ther.* **2001**, *90*, 231−259.
(2) Hackling, A. E.; Stark, H. Dopamine D3 receptor ligands with antagonist properties. *ChemBioChem* **2002**, *3*, 946−961.
(3) Carroll, F. I.; Howell, L. L.; Kuhar, M. J. Pharmacotherapies for treatment of cocaine abuse: preclinical aspects. *J. Med. Chem.* **1999**, *42*, 2721−2731.
(4) Montplaisir, J.; Nicolas, A.; Denesle, R.; Gomez-Mancilla, B. Restless legs syndrome improved by pramipexole: a double-blind randomized trial. *Neurology* **1999**, *52*, 938−943.
(5) van Vliet, L. A.; Tepper, P. G.; Dijkstra, D.; Damsma, G.; Wikstrom, H.; Pugsley, T. A.; Akunne, H. C.; Heffner, T. G.; Glase, S. A.; Wise, L. D. Affinity for dopamine D_2, D_3 and D_4 receptors of 2-aminotetralins. Relevance of D_2 agonist binding for determination of receptor subtype selectivity. *J. Med. Chem.* **1996**, *39*, 4233−4237.
(6) Malmberg, A.; Nordvall, G.; Johansson, A. M.; Mohell, N.; Hacksell, U. Molecular basis for the binding of 2-aminotetralins to human dopamine D_{2A} and D_3 receptors. *Mol. Pharmacol.* **1994**, *46*, 299−312.
(7) Pilla, M.; Perachon, S.; Sautel, F.; Garrido, F.; Mann, A.; Wermuth, C. G.; Schwartz, J.-C.; Everitt, B. J.; Sokoloff, P. Selective inhibition of cocaine-seeking behaviour by a partial dopamine D_3 receptor agonist. *Nature* **1999**, *400*, 371−375.
(8) Wicke, K.; Garcia-Ladona, J. The dopamine D3 receptor partial agonist, BP 897, is an antagonist at human dopamine D3 receptors and at rat somatodendritic dopamine D3 receptors. *Eur. J. Pharmacol.* **2001**, *424*, 85−90.
(9) Bettinetti, L.; Schlotter, K.; Hubner, H.; Gmeiner, P. Interactive SAR studies: rational discovery of super-potent and highly selective dopamine D_3 receptor antagonists and partial agonists. *J. Med. Chem.* **2002**, *45*, 4594−4597.
(10) Homan, E. J.; Wikstrom, H. V.; Grol, C. J. Molecular modeling of the dopamine D_2 and serotonin $5\text{-}HT_{1A}$ receptor binding modes of the enantiomers of 5-OMe-BPAT. *Bioorg. Med. Chem.* **1999**, *7*, 1805−1820.
(11) Teeter, M. M.; Froimowitz, M.; Stec, B.; DuRand, C. J. Homology Modeling of the dopamine D_2 receptor and its testing by docking of agonists and tricyclic antagonists. *J. Med. Chem.* **1994**, *37*, 2874−2888.
(12) Malmberg, A.; Nordvall, G.; Johansson, A. M.; Mohell, N.; Hacksell, U. Molecular basis for the binding of 2-aminotetralins to human dopamine D_{2A} and D_3 receptors. *Mol. Pharmacol.* **1994**, *46*, 299−312.
(13) Trumpp-Kallmeyer, S.; Hoflack, J.; Bruinvels, A.; Hibert, M. Modeling of G-protein-coupled receptors: application to dopamine, adrenaline, serotonin, acetylcholine, and mammalian opsin receptors. *J. Med. Chem.* **1992**, *35*, 3448−62.
(14) Livingstone, C. D.; Strange, P. G.; Naylor, L. H. Molecular modeling of D_2-like dopamine receptors. *Biochem. J.* **1992**, *287*, 277−282.
(15) Dahl, S. G.; Edvardsen, O.; Sylte, I. Molecular dynamics of dopamine at the D_2 receptor. *Proc. Natl. Acad. Sci. U.S.A.* **1991**, *88*, 8111−8115.
(16) Palczewski, K.; Kumasaka, T.; Hori, T.; Behnke, C. A.; Motoshima, H.; Fox, B. A.; Trong, I. L.; Teller, D. C.; Okada, T.; Stenkamp, R. E.; Yamamoto, M.; Miyano, M. Crystal structure of rhodopsin: a G protein-coupled receptor. *Science* **2000**, *289*, 739−745.
(17) Teller, D. C.; Okada, T.; Behnke, C. A.; Palczewski, K.; Stenkamp, R. E. Advances in determination of a high-resolution three-dimensional structure of rhodopsin, a model of G-protein-coupled receptors (GPCRs). *Biochemistry* **2001**, *40*, 7761−7772.
(18) Luecke, H.; Schobert, B.; Lanyi, J. K.; Spudich, E. N.; Spudich, J. L. Crystal structure of sensory rhodopsin II at 2.4 angstroms: insights into color tuning and transducer interaction. *Science* **2001**, *293*, 1499−1503.
(19) Okada, T.; Fujiyoshi, Y.; Silow, M.; Navarro, J.; Landau, E. M.; Shichida, Y. Functional role of internal water molecules in rhodopsin revealed by X-ray crystallography. *Proc. Natl. Acad. Sci. U.S.A.* **2002**, *99*, 5982−5987.
(20) Royant, A.; Nollert, P.; Edman, K.; Neutze, R.; Landau, E. M.; Pebay-Peyroula, E.; Navarro, J. X-ray structure of sensory rhodopsin II at 2.1-A resolution. *Proc. Natl. Acad. Sci. U.S.A.* **2001**, *98*, 10131−10136.
(21) Efremov, R. G.; Nolde, D. E.; Vergoten, G.; Arseniev, A. S. A solvent model for simulations of peptides in bilayers. II. Membrane-spanning α-helices. *Biophys. J.* **1999**, *76*, 2460−2471.
(22) Botelho, A. V.; Gibson, N. J.; Thurmond, R. L.; Wang, Y.; Brown, M. F. Conformational energetics of rhodopsin modulated by nonlamellar-forming lipids. *Biochemistry* **2002**, *41*, 6354−6368.

(23) Baldwin, J. M.; Schertler, G. F. X.; Unger, V. M. An Alpha-carbon template for the transmembrane helices in the rhodopsin family of G-protein-coupled receptors. *J. Mol. Biol.* **1997**, *272*, 144−164.
(24) van Leeuwen, D. H.; Eisenstein, J.; O'Malley, K.; MacKenzie, R. G. Characterization of a chimeric human dopamine D_3/D_2 receptor functionally coupled to adenylyl cyclase in Chinese hamster ovary cells. *Mol. Pharmacol.* **1995**, *48*, 344−351.
(25) Filteau, F.; Veilleux, F.; Levesque, D. Effects of reciprocal chimeras between the C-terminal portion of third intracellular loops of the human dopamine D_2 and D_3 receptors. *FEBS Lett.* **1999**, *447*, 251−256.
(26) Heller, H.; Schaefer, M.; Schulten, K. Molecular dynamics simulation of a bilayer of 200 lipids in the gel and in the liquid-crystal phases. *J. Phys. Chem.* **1993**, *97*, 8343−8360.
(27) Brooks, B. R.; Bruccoleri, R. E.; Olafson, B. D.; States, D. J.; Swaminathan, S.; Karplus, M. CHARMM: A Program for Macromolecular Energy, Minimization, and Dynamics Calculations. *J. Comput. Chem.* **1983**, *4*, 187−217.
(28) Shi, L.; Javitch, J. A. The binding site of aminergic G protein-coupled receptors: the transmembrane segments and second extracellular loop. *Annu. Rev. Pharmacol. Toxicol.* **2002**, *42*, 437−467.
(29) Ballesteros, J. A.; Shi, L.; Javitch, J. A. Stuctural mimicry in G protein-coupled receptors: implications of the high-resolution of rhodopsin for structure−function analysis of rhodopsin-like receptors. *Mol. Pharmacol.* **2001**, *60*, 1−19.
(30) Cho, W.; Taylor, L. P.; Mansour, A.; Akil, H. Hydrophobic residues of the D_2 dopamine receptor are important for binding and signal transduction. *J. Neurochem.* **1995**, *65*, 2105−15.
(31) Sheikh, S. P.; Zvyaga, T. A.; Lichtarge, O.; Sakmar, T. P.; Bourne, H. R. Rhodopsin activation blocked by metal-ion-binding sites linking transmembrane helices C and F. *Nature* **1996**, *383*, 347−350.
(32) Sheikh, S. P.; Vilardarga, J. P.; Baranski, T. J.; Lichtarge, O.; Iiri, T.; Meng, E. C.; Nissenson, R. A.; Bourne H. R. Similar structures and shared switch mechanisms of the β2-adrenoceptor and the parathyroid hormone receptor. Zn(II) bridges between helices III and VI block activation. *J. Biol. Chem.* **1999**, *274*, 17033−41.
(33) Jensen, A. D.; Guarnieri, F.; Rasmussen, S. G. F.; Asmar, F.; Ballesteros, J. A.; Gether, U. Agonist-induced conformational changes at the cytoplasmic side of transmembrane segment 6 in the β2 adrenergic receptor mapped by site-selective fluorescent labeling. *J. Biol. Chem.* **2001**, *276*, 9279−9290.
(34) Farrens, D. L.; Altenbach, C.; Yang, K.; Hubbell, W. L., Khorana, H. G. Requirement of rigid-body motion of transmembrane helices for light activation of rhodopsin. *Science* **1996**, *274*, 768−770.
(35) Ballesteros, J. A.; Jensen, A. D.; Liapakis, G.; Rasmussen, S. G. F.; Shi, L.; Gether, U.; Javitch, J. A. Activation of the β2-adrenergic receptor involves disruption of an ionic lock between the cytoplasmic ends of transmembrane segments 3 and 6. *J. Biol. Chem.* **2001**, *276*, 29171−29177.
(36) Gether, U.; Lin, S.; Ghanouni, P.; Ballesteros, J. A.; Weinstein, H.; Kobilka, B. K. Agonists induce conformational changes in thransmembrane domains III and Vi of the β2 adrenoceptor. *EMBO J.* **1997**, *16*, 6737−6747.
(37) Javitch, J. A.; Fu, D.; Liapakis, G.; Chen, J. Constitutive activation of the β2 adrenergic receptor alters the orientation of its sixth membrane-spanning segment. *J. Biol. Chem.* **1997**, *272*, 18546−18549.
(38) Shi, L.; Simpson, M. M.; Ballesteros, J. A.; Javitch, J. A. The first transmembrane segment of the dopamine D_2 receptor: Accessibility in the binding site crevice and position in the transmembrane bundle. *Biochemistry* **2001**, *40*, 12339−12348.
(39) Javitch, J. A.; Fu, D.; Chen, J.; Karlin, A. Mapping the binding-site crevice of the dopamine D_2 receptor by the substituted-cysteine accessibility method. *Neuron* **1995**, *14*, 825−831.
(40) Javitch, J. A.; Fu, D.; Chen, J. Residues in the fifth membrane-spanning segment of the dopamine D_2 receptor exposed in the binding-site crevice. *Biochemistry* **1995**, *34*, 16433−39.
(41) Javitch, J. A.; Fu, D.; Chen, J. Differentiating dopamine D_2 ligands by their sensitivities to modification of the cysteine exposed in the binding-site crevice. *Mol. Pharmacol.* **1996**, *49*, 692−698.
(42) Javitch, J. A.; Ballesteros, J. A.; Weinstein, H.; Chen, J. A cluster of aromatic residues in the sixth membrane-spanning segment of the dopamine D_2 receptor is accessible in the binding-site crevice. *Biochemistry* **1998**, *37*, 998−1006.
(43) Javitch, J. A.; Ballesteros, J. A.; Chen, J.; Chiappa, V.; Simpson, M. M. Electrostatic and aromatic microdomains within the binding-site crevice of the D_2 receptor: contributions of the second membrane-spanning segment. *Biochemistry* **1999**, *38*, 7961−68.
(44) Javitch, J. A.; Shi, L.; Simpson, M. M.; Chen, J.; Chiappa, V.; Visiers, I.; Weinstein, H.; Ballesteros, J. A. The fourth transmembrane segment of the dopamine D_2 receptor: accessibility in the binding-site crevice and position in the transmembrane bundle. *Biochemistry* **2000**, *39*, 12190−99.
(45) Fu, D.; Ballesteros, J. A.; Weinstein, H.; Chen, J.; Javitch, J. A. Residues in the seventh membrane-spanning segment of the dopamine D_2 receptor accessible in the binding-site crevice. *Biochemistry* **1996**, *35*, 11278−85.
(46) Vanhauwe, J. F. M.; Fraeyman, N.; Francken, B. J. B.; Luyten, W. H. M. L.; Leysen, J. E. Comparison of the ligand binding and signaling properties of human dopamine D_2 and D_3 receptors in Chinese hamster ovary cells. *J. Pharmacol. Exp. Ther.* **1999**, *290*, 908−916.
(47) Malmberg, M.; Mohell, N. Agonist and inverse agonist activity at the dopamine D_3 receptor measured by guanosine 5′-gamma-thio-triphosphate-35S- binding. *J. Pharmacol. Exp. Ther.* **1998**, *285*, 119−126.
(48) Burris, K. D.; Pacheco, M. A.; Filtz, T. M.; Kung, M.-P.; Kung, H. F.; Molinoff, P. B. Lack of discrimination by agonists for D_2 and D_3 dopamine receptors. *Neuropsychopharmacology* **1995**, *12*, 335−345.
(49) Cerius^2, a molecular modeling system, supplied by Accelrys Inc., San Diego, CA.
(50) Sartania, N.; Strange, P. G. Role of conserved serine residues in the interaction of agonists with D_3 dopamine receptors. *J. Neurochem.* **1999**, *72*, 2621−2624.
(51) Lundstrom, K.; Turpin, M. P.; Large, C.; Robertson, G.; Thomas, P.; Lewell, X.-Q. Mapping of dopamine D_3 receptor binding site by pharmacological characterization of mutants expressed in CHO cells with the Semliki Forest virus system *J. Recept. Signal Transduct. Res.* **1998**, *18*, 133−150.
(52) Cotte, N.; Balestre, M. N.; Aumelas, A.; Mahe, E.; Phalipou, S.; Morin, D.; Hibert, M.; Manning, M.; Durroux, T.; Barberis, C.; Mouillac, B. Conserved aromatic residues in the transmembrane region VI of the V1a vasopressin receptor differentiate agonist vs antagonist ligand binding, *Eur. J. Biochem.* **2000**, *267*, 4253−63.
(53) Chen, S.; Xu, M.; Lin, F.; Lee, D.; Riek, P.; Graham, R. M. Phe310 in transmembrane VI of the alpha1B-adrenergic receptor is a key switch residue involved in activation and catecholamine ring aromatic bonding. *J. Biol. Chem.* **1999**, *274*, 16320−30.
(54) Noda, K.; Saad, Y.; Karnik, S. S. Interaction of Phe8 of angiotensin II with Lys199 and His256 of AT1 receptor in agonist activation. *J. Biol. Chem.* **1995**, *270*, 28511−14.
(55) Spalding, T. A.; Burstein, E. S.; Henderson, S. C.; Ducote, K. R.; Brann, M. R. Identification of a ligand-dependent switch within a muscarinic receptor. *J. Biol. Chem.* **1998**, *273*, 21563−68.
(56) Granas, C.; Nordvall, G.; Larhammar, D. Mutagenesis of the human 5-HT1B receptor: differences from the closely related 5-HT1A receptor and the role of residue F331 in signal transduction. *J. Recept. Signal. Transduct. Res.* **1998**, *18*, 225−241.
(57) Choudhary, M. S.; Craigo, S.; Roth, B. L. A single point mutation (Phe340→Leu340) of a conserved phenylalanine abolishes 4-[^{125}I]-iodo-(2,5-dimethoxy)-phenylisopropylamine and [^{3}H]mesulergine but not [^{3}H]ketanserin binding to 5-hydroxytryptamine2 receptors. *Mol. Pharmacol.* **1993**, *43*, 755−761.
(58) Kurogi, Y.; Guner, O. F. Pharmacophore modeling and three-dimensional database searching for drug design using catalyst. *Curr. Med. Chem.* **2001**, *8*, 1035−1055.
(59) Milne, G. W.; Nicklaus, M. C.; Wang, S. Pharmacophores in drug design and discovery. *SAR QSAR Environ. Res.* **1998**, *9*, 23−38.
(60) Wang, S.; Sakamuri, S.; Enyedy, I. J.; Kozikowski, A. P.; Deschaux, O.; Bandyopadhyay, B. C.; Tella, S. R.; Zaman, W. A.; Johnsons, K. M. Discovery of a novel dopamine transporter inhibitor, 4-hydroxy-1-methyl-4-(4-methylphenyl)-3-piperidyl 4-methylphenyl ketone, as a potential cocaine antagonist through 3D-database pharmacophore searching. Molecular modeling, structure−activity relationships, and behavioral pharmacological studies. *J. Med. Chem.* **2000**, *43*, 351−360.
(61) Betti, L.; Botta, M.; Corelli, F.; Floridi, M.; Giannaccini, G.; Maccari, L.; Manetti, F.; Strappaghetti, G.; Tafi, A.; Corsano, S. Alpha(1)-adrenoceptor antagonists. 4. Pharmacophore-based design, synthesis and biological evaluation of new imidazo-, benzimidazo- and indoloarylpiperazine derivatives. *J. Med. Chem.* **2002**, *45*, 3603−3611.
(62) Langer, T.; Hoffmann, R. D. Virtual screening: an effective tool for lead structure discovery? *Curr. Pharm. Des.* **2001**, *7*, 509−527.
(63) Enyedy, I. J.; Ling, Y.; Nacro, K.; Tomita, Y.; Wu, X.; Cao, Y.; Guo, R.; Li, B.; Zhu, X.; Huang, Y.; Long, Y. Q.; Roller, P. P.; Yang, D.; Wang, S. Discovery of small-molecule inhibitors of Bcl-2 through structure-based computer screening. *J. Med. Chem.* **2001**, *44*, 4313−4324.

(64) Gradler, U.; Gerber, H.-D.; Goodenough-Lashua, D. M.; Garcia, G. A.; Ficner, R.; Reuter, K.; Stubbs, M. T.; Klebe, G. A new target for shigellosis: Rational design and crystallographic studies of inhibitors of tRNA-guanine transglycosylase. *J. Mol. Biol.* **2001**, *306*, 455−467.
(65) Sarmiento, M.; Wu, L.; Keng, Y.-F.; Song, L.; Luo, Z.; Huang, Z.; Wu, G.-Z.; Yuan, A. K.; Zhang, Z.-Y. *J. Med. Chem.* **2000**, *43*, 146−155.
(66) Perola, E.; Xu, K.; Kollmeyer, T. M.; Kaufmann, S. H.; Prendergast, F. G.; Pang, Y.-P. Successful Virtual screening of a chemical database for farnesyltransferase inhibitor leads. *J. Med. Chem.* **2000**, *43*, 401−408.
(67) Iwata, Y.; Arisawa, M.; Hamada, R.; Kita, Y.; Mizutani, M. Y.; Tomioka, N.; Itai, A.; Miyamoto, S. Discovery of novel aldose reductase inhibitors using a protein structure-based approach: 3D-database search followed by design and synthesis. *J. Med. Chem.* **2001**, *44*, 1718−1728.
(68) Debnath, A. K.; Radigan, L.; Jiang, S. Structure-based identification of small molecule antiviral compounds targeted to the gp41 core structure of the human immunodeficiency virus type 1. *J. Med. Chem.* **1999**, *42*, 3203−3209.
(69) Quanta, a molecular modeling system, is supplied by Molecular Simulations Inc., San Diego, CA.
(70) Milne, G. W. A.; Nicklaus, M. C.; Driscoll, J. S.; Wang, S.; Zaharevitz, D. W. The NCI Drug Information System 3D Database, *J. Chem. Inf. Comput. Sci.* **1994**, *34*, 1219−1224.
(71) Chem-X is a product of Chemical Design Ltd., 7 West Way, Oxford OX2 0JB, England.
(72) Sonesson, C.; Lin, C.-H.; Hansson, L.; Waters, N.; Svensson, K.; Carlsson, A.; Smith, M. W.; Wikstrom, H. Substituted (*S*)-Phenylpiperidines and rigid congeners as preferential dopamine autoreceptor antagonists: synthesis and structure−activity relationships. *J. Med. Chem.* **1994**, *37*, 2735−53.
(73) Cheng, Y.; Prussoff, W. H. Relationship between the inhibition constant (Ki) and the concentration of inhibitor which causes 50% inhibition (IC50) of an enzymatic reaction. *Biochem. Pharmacol.* **1973**, *22*, 3099−3108.
(74) Terp, G. E.; Johansen, B. N.; Christensen, I. T.; Jorgensen, F. S. A new concept for multidimensional selection of ligand conformations (MultiSelect) and multidimensional scoring (MultiScore) of protein−ligand binding affinities. *J. Med. Chem.* **2001**, *44*, 2333−2343.
(75) MacKerell, A. D., Jr.; Bashford, D.; Bellott, M.; Dunbrack, R. L., Jr.; Evanseck, J. D.; Field, M. J.; Fischer, S.; Gao, J.; Guo, H.; Ha, S.; Joseph-McCarthy, D.; Kuchnir, L.; Kuczera, K.; Lau, F. T. K.; Mattos, C.; Michnick, S.; Ngo, T.; Nguyen, D. T.; Prodhom, B.; Reiher, W. E., III; Roux, B.; Schlenkrich, M.; Smith, J. C.; Stote, R.; Straub, J.; Watanabe, M.; Wiorkiewicz-Kuczera, J.; Yin, D.; Karplus, M. All-atom empirical potential for molecular modeling and dynamics studies of proteins. *J. Phys. Chem. B* **1998**, *102*, 3586−3616.
(76) Feller, S. E.; Gawrisch, K.; MackKerell, A. D., Jr. Polyunsaturated fatty acids in lipid bilayers: intrinsic and environmental contributions to their unique physical properties. *J. Am. Chem. Soc.* **2002**, *124*, 318−326.
(77) Carpenter, G. A.; Grossberg, S. ART 2: Self-organization of stable category recognition codes for analog input patterns. *Appl. Opt.* **1987**, *26*, 4919−4930.
(78) Karpen, M. E.; Tobias, D. T.; Brooks, C. L., III Statistical clustering techniques for analysis of long molecular dynamics trajectories. I: Analysis of 2.2 ns trajectories of YPGDV. *Biochemistry* **1993**, *32*, 412−420.
(79) Godden, J. W.; Xue, L.; Bajorath, J. Combinatorial Preferences Affect Molecular Similarity/Diversity Calculations Using Binary Fingerprints and Tanimoto Coefficients. *J. Chem. Inf. Comput. Sci.* **2000**, *40*, 163−166.
(80) Freedman, B. S.; Patel, S.; Marwood, R.; Emms, F.; Seabrook, G. R.; Knowles, M. R.; McAllister, G. Expression and pharmacological characterization of the human D_3 dopamine receptor. *J. Pharmacol. Exp. Ther.* **1994**, *268*, 417−426.
(81) Yang, D.; Kefi, S.; Audinot, V.; Millan M.-J.; Langlois, M. Benzamides derived from 1,2-diaminocyclopropane as novel ligands for human D_2 and D_3 dopamine receptors. *Bioorg. Med. Chem.* **2000**, *8*, 321−327.
(82) Mewshaw, R. E.; Kavanagh, J.; Stack, G.; Marquis, K. L.; Shi, X.; Kagan, M. Z.; Webb, M. B.; Katz, A. H.; Park, A.; Kang, Y. H.; Abou-Gharbia, M.; Scerni, R.; Wasik, T.; Cortes-Burgos, L.; Spangler, T.; Brennan, J. A.; Piesla, M.; Mazandarani, H.; Cockett, M. I.; Ochalski, R.; Coupet, J.; Andree, T. H. New generation dopaminergic agents. 1. Discovery of a novel scaffold which embraces the D_2 agonist pharmacophore. Structure−activity relationships of a series of 2-(aminomethyl)chromans. *J. Med. Chem.* **1997**, *40*, 4235−4256.
(83) Audinot, V.; Newman-Tancredi, A.; Gobert, A.; Rivet, J.-M.; Brocco, M.; Lejeune, F.; Gluck, L.; Desposte, I.; Bervoets, K.; Dekeyne, A.; Millan, M. J. A comparative in vitro and in vivo pharmacological characterization of the novel dopamine D_3 receptor antagonists (+)-S14297, nafadotride, GR103, 691 and U99194. *J. Pharmacol. Exp. Ther.* **1998**, *287*, 187−197.
(84) Alberts, G. L.; Pregenzer, J. F.; Im, W. B. Contributions of cysteine 114 of the human D_3 dopamine receptor to ligand binding and sensitivity to external oxidizing agents. *Br. J. Pharmacol.* **1998**, *125*, 705−710.
(85) Millan, M. J.; Peglion, J. L.; Rivet, J. M.; Brocco, M.; Gober, A.; Newman-Tancredi, A.; Dacquet, C.; Bervoets, K.; Girardon, S. et al., Functional correlates of dopamine D_3 receptor activation in the rat in vivo and their modulation by the selective antagonist, (+)-S14297: 1. Activation of postsynaptic D_3 receptors mediates hypothermia, whereas blockade of D_2 receptors elicits prolactin secretion and catalepsy. *J. Pharmacol. Exp. Ther.* **1995**, *275*, 885−898.
(86) Newman-Tancredi, A.; Audinot, V.; Jacques, V.; Peglion, J. L.; Millan, M. J. [^{3}H](+)S14297: A novel, selective radioligand at cloned human dopamine D_3 receptors. *Neuropharmacology* **1995**, *34*, 1693−1696.
(87) Nader, M. A.; Green, K. L.; Luedtke, R. R.; Mach, R. H. The effects of benzamide analogues on cocaine self-administration in rhesus monkeys. *Psychopharmacology* **1999**, *147*, 143−152.
(88) Millan, M. J.; Gobert, A.; Newman-Tancredi, A.; Lejeune, F.; Cussac, D.; Rivet, J.-M.; Audinot, V.; Dubuffet, T.; Lavielle, G. S33084, a novel, potent, selective and competitive antagonist at dopamine D_3 receptors: I. Receptorial, electrophysiological and neurochemical profile compared with GR218,231 and L741,626. *J. Pharmacol. Exp. Ther.* **2000**, *293*, 1048−1062.
(89) Pugsley, T. A.; Davis, M. D.; Akunne, H. C.; Cooke, L. W.; Whetzel, S. Z.; MacKenzie, R. G.; Shih, Y. H.; van Leeuwen, D. H.; DeMattos, S. B.; Georgic, L. M. CI-1007, a dopamine partial agonist and potential antipsychotic agent. I. Neurochemical effects. *J. Pharmacol. Exp. Ther.* **1995**, *274*, 898−911.
(90) Sonesson, C.; Waters, N.; Svensson, K.; Carlsson, A.; Smith, M. W.; Piercey, M. F.; Meier, E.; Wikstrom, H. Substituted 3-phenylpiperidines: new centrally acting dopamine autoreceptor antagonists. *J. Med. Chem.* **1993**, *36*, 3188−3196.
(91) Stjernlof, P.; Lin, C.-H.; Sonesson, C.; Svensson, K.; Smith, M. W. (Dipropylamino)-tetrahydronaphthofurans: centrally acting serotonin agonists and dopamine agonists-antagonists. *Bioorg. Med. Chem. Lett.* **1997**, *7*, 2759−2764.

JM030085P